Ana Garcia Corrêa

CLIMATOLOGIA DOS VENTOS E POTENCIAL EÓLICO OFFSHORE DE SANTA CATARINA

Dissertação submetida ao Programa de Pós-Graduação em Oceanografia da Universidade Federal de Santa Catarina para obtenção do Grau de Mestre em Oceanografia.
Orientador: Prof. Dr. Felipe Mendonça Pimenta

Florianópolis

2018

ANA GARCIA CORRÊA

CLIMATOLOGIA DOS VENTOS E POTENCIAL EÓLICO OFFSHORE DE SANTA CATARINA

Florianópolis, 27 de Agosto de 2018.

_____
Prof. Dr. Antônio Henrique da Fontoura Klein
Coordenador do Programa de Pós-Graduação em Oceanografia

Banca Examinadora:

_____
Prof. Dr. Felipe Mendonça Pimenta
Orientador
Universidade Federal de Santa Catarina

_____
Profa. Dra Carla de Abreu D'Aquino.
Universidade Federal de Santa Catarina

_____
Prof. Dr. Renato Ramos da Silva
Universidade Federal de Santa Catarina

'Sempre que me acontece
Alguma coisa importante,
Está ventando'
(Érico Verissimo em *O Tempo e o Vento*.)

AGRADECIMENTOS

Ao meu orientador, Prof. Felipe, por todos conhecimentos divididos.

Aos professores Carla e Renato, pela disponibilidade em participar da banca e colaborarem com o trabalho desde a avaliação do projeto.

A família, mãe e pai, mana e Vini por todo o suporte e amor.

As minhas tias e tio que me acolheram em Floripa, junto com as primas irmãzinhas.

Aos amigos do LabDINO pelos muitos litros de mate compartilhados e companheirismo. Obrigada em especial ao Micael, João, Luis, Pam, Arthur, César, Anthea e Bagé que salvaram em vários momentos.

Ao seu Luis pela segurança e os bons dias mais simpáticos. Ao Milano por ajudar em todos os momentos possíveis. Aos meus colegas e amigos que trilharam essa caminhada junto.

RESUMO

A energia eólica é a fonte alternativa que mais cresceu no Brasil, mas ainda não há parques eólicos instalados *offshore*. Este trabalho avaliou os recursos eólicos da região costeira e oceânica do estado de Santa Catarina através da análise de 32 anos de dados do modelo WRF (Weather Research and Forecasting) e de 1 ano de medições através da tecnologia LiDAR (Light Detection and Ranging). Os objetivos foram identificar as áreas de maior potencial para exploração de energia e a viabilidade através da análise batimétrica. Os ventos marítimos foram mais intensos que os terrestres, com velocidades médias sazonais chegando a 9 ms^{-1} no sul do estado. Em comparação entre as áreas costeiras e oceânicas, levando em consideração altitude e profundidades, o potencial oceânico até 50 m, foi de 39 GW. A densidade de potência no sul do estado, nos períodos de inverno e primavera foram de 90 e 1400 Wm^2 respectivamente. Os ventos predominantes foram de nordeste e sudeste. Os dados da modelagem corroboraram aos do LiDAR, mesmo sendo referentes a períodos diferentes.

Palavras-Chave: Energia Eólica Offshore, Ventos oceânicos, Climatologia, Santa Catarina

ABSTRACT

Wind energy is the fastest growing alternative source in Brazil, but there are still no offshore wind farms. This work evaluated the wind resources of the coastal and oceanic region of the state of Santa Catarina through the analysis of 32 years of WRF (Weather Research and Forecasting) and 1 year of in situ measurements using LiDAR (Light Detection and Ranging). The objectives were to identify the greatest potential areas for energy exploration and viability through bathymetric analysis. The sea winds were more intense than the terrestrial ones, with seasonal average speeds reaching 9 ms^{-1} in the south of the state. In comparison between the coastal and oceanic areas, taking into account altitude and depths, the oceanic potential up to 50 m, was 39 GW. The power density in the south of the state, in the winter and spring periods, were 90 and 1400 Wm^2 respectively. The prevailing winds were northeast and southeast. Modeling data corroborated those of LiDAR, even at different times.

Keywords: Offshore Wind energy, Ocean Winds, Climatology, Santa Catarina

Figure 5 Climatological seasonal fields (1979-2010) of wind power density at the height of 90 m above the surface. The bathymetric contours of 30, 50, and 100 m are identified. The panels correspond to the **(a)** Summer (Dec-Jan-Feb), **(b)** Fall (Mar-Apr-May), **(c)** Winter (Jun-Jul-Aug), and **(d)** Spring (Sep-Oct-Nov) periods. The color scale represents the power density in Wm^{-2}.

Figure 6 Climatological seasonal fields (1979-2010) of practical power generated by a 3-MW Vestas turbine, calculated from winds at the height of 90 m above the surface. The bathymetric contours of 30, 50, and 100 m are identified. The panels correspond to the **(a)** Summer (Dec-Jan-Feb), **(b)** Fall (Mar-Apr-May), **(c)** Winter (Jun-Jul-Aug), and **(d)** Spring (Sep-Oct-Nov) periods. The color scale represents the power in kilowatts (kW).

Figure 7 Climatological seasonal fields (1979-2010) of practical power generated by a 8-MW Vestas turbine, calculated from winds at the height of 90 m above the surface. The bathymetric contours of 30, 50, and 100 m are identified. The panels correspond to the **(a)** Summer (Dec-Jan-Feb), **(b)** Fall (Mar-Apr-May), **(c)** Winter (Jun-Jul-Aug), and **(d)** Spring (Sep-Oct-Nov) periods. The color scale indicates the power in kilowatts (kW).

Figure 8 Spring climatological transects of wind intensity as a function of longitude and height. Left panels illustrate the average wind speed in the continental and oceanic regions for the North (N), Central (C) and South (S) sectors. The black continuous contours represent the topography and bathymetry. The panels on the right illustrate the same North (N), Central (C) and South (S) sectors, with detail for the boundary layer between 0 and 150 m high relative to the land (or sea) surface. Vertical dashed lines indicate the coastline and the bay. The position of these sectors is shown in Figure 1a. The color scale represents the wind speed in ms^{-1}.

Figure 9 Mean vertical profiles derived from the modeling results at a 3-km resolution corresponding to the period between 1979-2010. The locations of these vertical profiles are identified in the North (N), Central (C), and South (S) sectors in Figure 1. In the lowest panel, we added LiDAR data from 2017 for comparison.

Figure 10 (a) LiDAR data throughout 2017. (b) WRF model results (1979-2010). Monthly variability of wind speed at the BOOA site. Jan (1), Feb (2), Mar (3), Apr (4), May (5), Jun (6), Jul (7), Aug (8), Sep (9), Oct (10), Nov (11), Dec (12). The central mark in each box is the median; the edges of the box correspond to the 25th and 75th percentiles. The dashes extend to the most extreme data points not considered outliers. Outliers are plotted as circles.

Figure 11 (a) WRF model results (1979-2010) at the BOOA site. **(b)** LiDAR data throughout 2017. Directional wind analysis by season. The percentages represent the number of occurrences in the wind direction and the colors represent the velocities in ms^{-1}.

Figure 12 (a) WRF model results (1979-2010) at the BOOA site. **(b)** LiDAR data throughout 2017. Seasonal analysis of directional power density for the summer (red line; Dec-Jan-Feb), fall (black line; Mar-Apr-May), winter (blue line; Jun-Jul-Aug), and spring (green line; Sep-Oct-Nov). The angles were aligned with the coastline (45°), represented by the thin black line that divides the plot into continental and ocean sectors in green and blue shades, respectively.

LISTA DE TABELAS

SUMÁRIO

1 INTRODUÇÃO GERAL

O cenário de aquecimento global, a necessidade de redução das emissões de gases do efeito estufa, o aumento populacional e a busca de segurança energética vem criando novas iniciativas de implementação de energias renováveis. Soma-se a estes problemas a crescente perda da confiança do público em relação à energia nuclear e os efeitos nocivos das fontes de energias convencionais fósseis sobre a saúde pública (Jacobson et al., 2015).

O Brasil, junto a 144 países assinou o Acordo de Paris em 2015, tratado das Nações Unidas, onde assumiu o compromisso de alcançar 45% de energias renováveis na composição da sua matriz energética até 2030.

A energia eólica *onshore* tem sido a modalidade renovável mais implementada no momento, devido a disponibilidade dos recursos e a tecnologia comercial já disponível a preços competitivos às outras fontes convencionais (Esteban et al, 2011). O vento vem sendo utilizado desde os primórdios em atividades econômicas como o bombeamento de água para irrigação, o uso de moinhos de grãos e a navegação. O primeiro gerador elétrico foi criado por Charles Brush em Ohio, EUA, no ano de 1888. Desde então houve uma revolução no conceito aerodinâmico e da eficiência dos geradores elétricos que cresceram significativamente em tamanho e potência nas últimas décadas (Manwell et al., 2009). Em 2007 a energia eólica alcançou pela primeira vez 1% da eletricidade gerada no mundo e atualmente a capacidade mundial de geração é 432 GW de potência (GWEC, 2015).

A primeira turbina eólica no mar, de 220 kW, foi criada na Suécia em 1990, localizada a 350 m da costa, sobre um tripé de 6 m de

profundidade. O primeiro projeto de fazenda eólica foi instalado na costa da Dinamarca em 1991. Atualmente turbinas variam de 2 a 7 MW e os maiores parques eólicos *offshore* estão no Reino Unido, Dinamarca e Bélgica, tendo a Europa cerca de 11 GW instalados (GWEC, 2015).

As vantagens da instalação de um parque eólico *offshore*, comparado ao continental, está em que o primeiro não possui limitações severas em termos de utilização do espaço e possui reduzido impacto visual; são reduzidos os impactos sonoros sociais devido a distância da costa; a superfície do mar tem baixa rugosidade e, assim é maior a densidade de potência do vento marítimo. Globalmente, a turbulência do vento também é inferior no mar, devido à ausência de barreiras. Assim, as turbinas não sofrem tanto desgaste, tendo um aumento em sua vida útil. A principal desvantagem é o custo mais alto do parque *offshore*, principalmente devido às fundações mais complexas e redes elétricas submersas.

Estudos apontam que com a fixação de um parque eólico *offshore* no fundo oceânico é possível gerar recifes artificiais, com agregação de peixes e áreas marinhas protegidas. Apesar de ter pontos negativos, como a interação com aves e ruídos sonoros para animais marinhos, as fazendas eólicas *offshore* tem capacidade de melhorar a biodiversidade de ambientes degradados (Inger et al, 2009). Projetos *offshore* precisam de operações complexas, com plataformas, turbinas, cabos, subestações, redes, transporte, dragagem e atividades de construção associadas. Essas atividades geram diferentes impactos nas fases de construção, operação e desativação; principalmente, ruído subaquático e impactos sobre a fauna local (Kaldellis et al, 2016). Outros estudos, como o de Kempton (2007) analisaram o quanto de CO_2 seria reduzido com parques eólicos

offshore em uma região específica do Atlântico Norte, sendo o potencial suficiente para atender a demanda de eletricidade e combustíveis de veículos leves local, reduzindo em 68% as emissões de CO_2. Os estudos mais atuais estão focando na influência das mudanças climáticas nos recursos naturais, principalmente vindos da água, vento e ondas (Pryor et al., 2013; Carvalho et al., 2017; Steiner et al., 2017;).

Para alcançar as metas do tratado da ONU, é importante ressaltar a capacidade do Brasil em gerar energia através dos recursos naturais renováveis, incentivado a muitas décadas. As hidrelétricas são responsáveis por 66% da energia gerada no Brasil. Ainda existe potencial a ser explorado, mas novos projetos estão encontrando entraves ambientais. A primeira turbina eólica brasileira foi instalada em 1992, no arquipélago de Fernando de Noronha. Os recursos continentais eólicos foram estimados em 143.5 GW, sendo a maior parte localizada no Nordeste e 15% na região Sul do país (Amarante et al, 2001). Os recursos da região oceânica entre 0 e 50 m são estimados em mais de 1.3 TW (Silva et al, 2015).

Segundo o Ministério de Minas e Energia Brasileiro (MME), em 2016 haviam 9 fabricantes de turbinas eólicas no Brasil, sendo um deles em SC, 4 de pás eólicas e 12 de torres. O boletim de junho de 2016 mostra que a geração eólica alcançou 6.18 GW em 370 fazendas eólicas *onshore*, sendo 6,2% da capacidade de geração nacional. Esse investimento reduziu em cerca de 16 milhões de toneladas as emissões de CO_2. Segundo o Plano Decenal de Expansão Energética 2024 (EPE, 2015), recursos de fontes renováveis como a eólica, biomassa e solar possuem taxa média anual de 10% de aumento da capacidade instalada

total e afirma que a geração eólica é um dos principais componentes para a expansão da matriz energética brasileira.

Estima-se que o potencial eólico do Brasil seja o suficiente para dez vezes sua demanda energética (Silva et al, 2015). Uma das dificuldades no desenvolvimento da energia eólica é a falta de linhas de transmissão suficientes nos locais de maior potência eólica. Segundo o Global Wind Report de 2015, não há planos a curto prazo para iniciar a energia eólica *offshore* no Brasil. As principais empresas do mercado brasileiro são CPFL Renováveis, Renova, Cubico, Eletrosul e Enel Green Power. A energia eólica brasileira foi impulsionada por um período de seca, onde as hidrelétricas estavam com baixos níveis. Essa fonte tem como principal vertente ser um complemento à energia hidrelétrica em períodos de baixa vazão dos rios, que tendem a ocorrer em períodos com maior potencial de vento. Em 1997 o Brasil possuía 1 MW instalado proveniente de energia eólica, em 2016 já estava com 7631 MW segundo o balanço energético da EPE (2017), com tendência de aumento constante, sendo de extrema importância acompanhamento do potencial de diversas áreas do país.

Na tabela 1 estão os dados da EPE (2017) de geração e capacidade instalada do estado, em comparação a região Sul e ao Brasil. A média de geração de Santa Catarina foi de 3.2 GW em 2016, o que vem aumentando na última década.

No estado de Santa Catarina existem 278 MW instalados segundo a CELESC. O maior parque eólico fica no município de Água Doce, na região oeste, com 9 usinas. As instalações começaram em 2002 com 23 torres e em 2017 estava com 109 torres. Em Bom Jardim da Serra há um parque com capacidade instalada de 93 MW com 62 torres, mas destas

apenas 8 estão em funcionamento. Parte da dificuldade de manutenção do parque está relacionada à sua baixa geração. Devido a sazonalidade dos ventos na região da serra, o potencial torna-se significativo apenas no inverno (D'Aquino 2018, com. pessoal). Em Santa Catarina há uma usina termelétrica com 857 MW de capacidade instalada, Complexo Jorge Lacerda, num total de 1070 MW dessa fonte no estado. A capacidade instalada de hidrelétricas no estado é de 4146 MW.

Segundo a CELESC, responsável por 93% do abastecimento do estado de SC, o consumo residencial foi de 5262 GWh em 2015 para 5439 GWh em 2016. Em 10 anos, o consumo aumentou 1638 GWh. O balanço energético nacional de 2017 apontou que no último trimestre do ano de 2016, o consumo total de energia elétrica no estado somou 5.559 GWh, um avanço de 1,5% no total de energia distribuída (mercado cativo e livre). O número de unidades consumidoras atendidas pela CELESC atingiu o total de 2.831.997 em dezembro de 2016, alta de 2,3% em relação ao mesmo período do ano anterior. A região sul, em 2016, representou 15.6 % do consumo residencial brasileiro.

Há poucos estudos sobre o mapeamento de ventos em regiões costeiras ou sobre o ambiente oceânico. Archer (2014), apontou a necessidade das medições de vento a diferentes níveis de altura usando torres meteorológicas, LiDARs e boias para melhor validar os modelos existentes e ajudar na assimilação de dados. Alterações na topografia, temperatura e rugosidade da superfície dificultam uma melhor compreensão espacial da estrutura dos ventos costeiros, faltando assim informações do potencial do estado de Santa Catarina. Em recente estudo, Colle (2016) utilizou medições de um LiDAR, torres

meteorológicas e de um avião não tripulado para descrição dos recursos *offshore*.

A maioria dos estudos de potencial eólico são baseados em dados de reanálises ou modelos de mesoescala. Neste trabalho há um comparativo entre essas fontes variadas de dados. Sempreviva (2008) revisou as metodologias aplicadas na avaliação do potencial eólico *offshore* da Europa e afirmou que os LiDARS permitem uma melhor caracterização na altura de 100m, melhor que as medições padrões que precisam de extrapolação vertical.

Alterações na temperatura do mar, temperatura do ar e rugosidade da superfície oceânica podem influenciar os fluxos de calor e momento da interface água-atmosfera (Capps et al, 2009). Por sua vez, tais fluxos impactam a estrutura da camada limite atmosférica. Assim o mapeamento dos ventos na altura de rotores de turbinas deve procurar levar tais parâmetros em consideração.

Em 2014 foi lançado o Atlas do Rio Grande do Sul, onde analisaram o potencial *offshore* até 50 m da zona econômica exclusiva e das lagoas, estimando em 80 GW a 100 m de altura, segundo análises com o modelo *WindMap*.

A Figura 1 ilustra o mapeamento dos ventos através de dados satelitários para diferentes estações do ano (Silva et al, 2015). Fica claro a presença de recursos significativos nas regiões Norte, Nordeste, Sudeste e Sul do Brasil. A produção de energia da região Sul é promissora, principalmente no período da primavera. O mapeamento ilustrado, entretanto, assumiu condições de uma atmosfera neutra para extrapolação vertical dos ventos.

A principal influência sobre os ventos de superfície na Região Sul do Brasil é o sistema de alta pressão do Atlântico Sul. Este padrão está em todas as estações, mas mais intenso no inverno. Esse centro de alta pressão produz ventos médios na superfície de leste ou nordeste, com intensidade fraca, podendo estar associado a divergência de ar a partir do centro de alta pressão. Essa divergência tende a ser mais forte junto a superfície devido ao atrito. Os movimentos sazonais do centro de alta pressão no oceano Atlântico Sul que determinam se os ventos em baixos níveis vão adentrar mais ou menos a costa brasileira (Cavalcanti, 2009).

Atualmente são três os tipos de fundações *offshore* disponíveis comercialmente: Monopile, Transicional e Flutuante. O sistema Monopile é indicado para águas rasas, até 30 m. Os sistemas Transicionais são para águas de até 60 m. Para águas mais profundas que 60 m o sistema flutuante é o mais indicado, mas está em fase de testes (Musial, 2006). A maior turbina eólica marinha será instalada em Fukushima, no Japão, com 220 m de altura e potência de 7 MW. Sua base é flutuante.

Nenhuma turbina extrai toda potência do vento, então é preciso calcular a densidade de potência do modelo a ser utilizado. Segundo Custódio (2013), uma turbina extrai cerca de 45% da potência total do vento[1]. A avaliação do potencial eólico leva em consideração a eficiência das turbinas e dados eólicos.

Neste trabalho, buscou-se melhorar esta estimativa através do cálculo do perfil do vento incluindo a densidade potencial na região. Calculou-se os campos de ventos climatológicos na altura das turbinas eólicas em maior resolução espacial para a região costeira do estado de

---

[1] O limite teórico de Betz é de 59.26%

Santa Catarina. Tais estimativas foram comparadas com observações de um LiDAR, instalado na região Sul do estado.

1.1 Perguntas de pesquisa

1) Qual o potencial eólico *offshore* de Santa Catarina?

2) A energia eólica *offshore* será capaz de atender a demanda energética do estado?

3) Qual o melhor local para a instalação de um parque eólico *offshore* na costa do estado?

1.2 Objetivo Geral

Descrever os recursos eólicos *offshore*, da região costeira de Santa Catarina, combinando medições in situ e climatológicos, contribuindo para o desenvolvimento da exploração de energias renováveis do Brasil.

1.3 Objetivos Específicos

• Mapear a distribuição da velocidade dos ventos na região costeira de Santa Catarina, através de dados in situ e climatológicos;

• Comparar os dados medidos pelo perfilador de ventos LiDAR com os dados do modelo WRF;

• Comparar o potencial energético dos ventos em área continental e em área *offshore* através do LiDAR;

• Avaliar o potencial eólico através do uso da batimetria e das características de turbinas modernas.

A hipótese testada foi de que o potencial eólico *offshore* é muito superior ao potencial eólico *onshore* de Santa Catarina, tendo capacidade de suprir a demanda elétrica do estado.

Santa Catarina Coastal and Offshore Wind Energy Potential

Este capítulo apresenta o conteúdo do artigo que compõe esta dissertação e foi submetido a revista *Brazilian Journal of Oceanography* em 27/07/2018. O conteúdo apresentado a seguir segue na íntegra ao enviado para a revista, alterada apenas a formatação do texto. O referido artigo é de autoria de Ana G. Côrrea, Felipe M. Pimenta, César Mattos Pires e Antonio H. F. Klein. A confirmação da submissão é apresentada na próxima página.

Artigo Submetido - Brazilian Journal of Oceanography

1 mensagem

Braz. j. oceanogr. - GNPapers <gnpapers@gnpapers.com.br>   27 de julho de 2018
Para: Ana Garcia Correa <anaagcorrea@gmail.com>

BRAZILIAN JOURNAL OF
OCEANOGRAPHY

Ilmo(a) Sr.(a)
Prof(a), Dr(a) Ana Garcia Correa

Número do artigo: 209
Seção: Artigo Completo

Informamos que recebemos o manuscrito "SANTA CATARINA COASTAL AND OFFSHORE WIND ENERGY POTENTIAL". Ele será enviado para apreciação dos revisores com vistas à publicação no(a) Brazilian Journal of Oceanography. Por favor, para qualquer comunicação futura sobre o referido manuscrito cite o número do artigo apresentado acima.

O(s) autor(es) declara(m) que o presente trabalho é inédito e o seu conteúdo não foi nem está sendo considerado para publicação em outro periódico brasileiro ou estrangeiro, impresso ou eletrônico.

Obrigado por submeter seu trabalho.

Atenciosamente,

Prof. Dr. Marcos César de Oliveira Santos
Editor-chefe

««« Enviado por GNPapers - Esta é uma mensagem automática - Por favor não responda este email »»»

2 Santa Catarina coastal and offshore wind energy potential

Ana G. Correa, Felipe M. Pimenta, César H. M. Pires, Antonio H. F. Klein

Graduate Program in Oceanography (PPGOceano). Center of Physical and Mathematical Sciences, Federal University of Santa Catarina, Trindade, Florianópolis, SC, 88040-900, Brazil.

Abstract

This study combines atmospheric modeling results with data acquired by a coastal LiDAR in order to describe the spatial structure and seasonal variability of winds in the coastal and offshore regions of Santa Catarina state, Brazil. The analyzed wind database refers to dynamic downscaling results from a Weather Research & Forecasting (WRF) model using Climate Forecast System Reanalysis (CRSR) global outputs from 1979 to 2010. Wind vertical profiles were obtained by a LiDAR on an urban continental area (Apr-Dec 2016) and over a fishing platform (from Dec 2016 to Dec 2017). Those results were combined with technical data from modern wind turbines and a digital terrain model to characterize the distribution of wind resources. Offshore winds were more intense and presented a lower vertical shear than the coastal continental winds. Winds in the summit of the Serra do Mar mountain range presented significant potential, comparable to the oceanic winds. Prevailing winds are from the northeast and southwest directions. Winds in the south of the state were more intense, what suggests the presence of an offshore low-level jet along the Santa Marta Cape and Araranguá. The seasonality and vertical structure of LiDAR data corroborated with

the numerical modeling results, even though it covered a distinct period. Between 0 and 30 m deep, the offshore wind potential was estimated to lie between 10 and 16 GW.

1. Introduction

The use of ocean renewable energy sources is an activity not yet explored in Brazil. Among the available forms are the tidal energy, wind-generated waves, oceanic thermal energy, large-scale currents, and wind energy (Charlier & Justus, 1990; Boyle, 2004).

The offshore wind energy is one of the most promising ways to exploit ocean energy in the coming years. The technology of wind turbines is mature. Their foundation allows the installation of turbines fixed to the seafloor between 0 and 50 m deep (Rodrigues et al., 2015). Floating technology is at a demonstration stage and the first wind farm off the Scottish coast has five 6 MW turbines installed between 95 and 120 m deep (Hywind, 2017).

Offshore wind energy currently has 18 GW of capacity installed worldwide. The majority of projects are located in Europe, but also in China, South Korea, Japan, Taiwan, and most recently in the United States (GWEC, 2017). On the one hand, projects are stimulated by the absence of promising continental areas to build new continental wind farms, but they are also motivated by the higher quality of winds, which without topographical barriers have higher energy density and less turbulence over the oceans (Pryor and Barthelmie, 2001; Garvine and Kempton, 2008; Manwell et al, 2009).

The practical potential of the offshore resource is higher than the current human consumption of electricity (IPCC, 2011; Archer and Jacobson, 2005; Lu et al., 2009; Capps and Zender, 2010). Winds also have a global distribution; many promising sites of energy generation are located near the consumption centers (Jacobson et al., 2017). In Europe, the USA, and Asia, the implementation of "super-grids" has been discussed, which would connect the distribution of energy produced by wind farms and other renewable sources over great geographic distances (Kempton et al., 2010; Rodrigues et al., 2015). In Brazil, wind energy has been traditionally explored in continental regions, corresponding to 12.7 GW (7.8%) of installed capacity (ANEEL, 2017). Amarante et al. (2001) estimated the Brazilian terrestrial potential at 143.5 GW at the height of 50 m turbines. Recent estimates have suggested a continental potential of 880 GW at 100 m high (FAPESP, 2016). The offshore potential was mapped with satellite data by Pimenta et al. (2008), Ortiz and Kampel (2011), and Silva et al. (2015). In a more recent evaluation in which the Blended Sea Winds (Zhang et al., 2009) database was used and the atmospheric stability was considered, Pimenta et al. (2018) estimated a national potential at 1.0 TW between 0 and 50 m deep and at 1.3 TW between 0 and 100 m. Climatological maps suggested that the northern (states of Amapá and Paraíba), northeastern (states of Piauí, Ceará, Rio Grande do Norte, and Paraíba), southeastern (states of Espírito Santo and Rio de Janeiro), and southern (states of Santa Catarina and Rio Grande do Sul) continental shelves are promising regions for offshore exploration (Fig. 7 from Pimenta et al., 2018). Satellite data from radiometers and scatterometers have excellent spatial (global ocean, free of sea ice) and temporal (1948-present) coverage,

which is appropriate for assessing the geographic distribution of resources over large oceanic distances – ranging from 10^2 to 10^3 km (Zhang et al., 2009; Liu et al., 2008; Pimenta et al., 2008; Capps and Zender, 2010; Silva et al., 2015; Pimenta et al., 2018)[2].The satellite spatial resolution of 0.25^o (~27 km), however, becomes a limitation in regional assessments when there is the need to describe the wind structure in detail at spatial scales varying from 10 to 10^2 km. The Santa Catarina coast, for example, is relatively extensive (about 450 km long) but relatively narrow, and the 50 m isobath is less than 25 km off the coast in certain localities. Topographical features are also located near the coast, potentially influencing the oceanic winds.

Archer (2014) highlights the current need to combine the information from towers, LiDAR profilers, and buoys with numerical modeling for the study of coastal winds. The strong gradients of temperature, roughness, and topography make the wind flow complex in the transition region of the ocean to the continental domain.

Atmospheric numerical models are increasingly being used as dynamic downscaling[3] tools. In this process, the results from global climate models (of lower spatial resolution, 0.5° or 1°) are used as boundary and initial conditions for numerical simulations of high spatial resolution (1/10°). As an example, Dvorak et al. (2010; 2013) used the Weather

[2] Another available satellite product refers to the SAR (Synthetic Aperture Radar) commercial images, which have great spatial resolution (~100 m), but poor temporal coverage (e.g. Monaldo et al., 2004; Hasager et al., 2006a,b).

[3] The "downscaling" term generically refers to the increase of spatial resolution using atmospheric data of lower resolution. The "dynamic downscaling" term refers to the spatial refinement performed by numerical models based on the equations of motion and conservation of properties.

Research & Forecasting model (WRF-ARW v3.2.1) at a 5 km resolution to estimate the offshore potential off the coast of the United States. Carvalho et al. (2017) compared satellite data (from scatterometers) with buoys and results from the WRF model (5 km resolution) for the Iberian Peninsula. The WRF model was also used in the assessment of winds in the Liaoning province in China (Li Ji-Hang et al., 2014), central region of Chile (Mattar and Guzmán-Ibarra, 2017a,b), and in the state of Paraíba, Brazil (Oliveira and Souza, 2017).

This work investigates the winds from the coastal region of the state of Santa Catarina (SC), one of the places with the greatest offshore wind potential in Brazil. We combined results from atmospheric modeling with data acquired by a LiDAR wind profiler. The modeling results consist of 32 years of data (1979-2010) from the SeaWind-StaCatarina product at a resolution of 3 km. This product refers to a dynamic downscaling performed with the WRF model (Menendez et al., 2011; 2014; Fernandez-Quiruelas et al., 2015; and Salvação et al., 2014) using the CFSR atmospheric reanalysis (Saha et al., 2010). LiDAR wind profiles were obtained in two locations in the south of SC: the first in the urbarn area of the Federal University of Santa Catarina (UFSC) Campus in Araranguá (April-December 2016) and the second campaign on a fishing platform in Balneário Arroio do Silva (from Dec 2016 to Dec 2017).

Results were complemented by a digital terrain model for topographic and bathymetric information and by the technical information of modern wind turbines. The data set allowed us to map wind resources, describing their seasonal variation and peculiar spatial structure in the ocean-continent transition region. The practical production of turbines

as well as the continental and oceanic energy potential were calculated, what surpasses the average consumption of the southern states of Brazil.

2. Database and methods

2.1 Digital terrain model

The study area covered the coastal region of the state of Santa Catarina, including parts of the Serra do Mar mountain range, the East, the General mountain range, and the plateau (Figure 1a). The digital terrain model was derived from the ETOPO1 (NGDC) database at a spatial resolution of 1/60°, displaying the relief with positive values for the altitude and negative values for the bathymetry (Amante et al., 2009). The ocean bathymetric contours of -30, -50, -100, -200, and -500 m are indicated in Figure 1a. The continental shelf is relatively wide in the northern domain and narrower in the south of the state close to 28.5° S. The contour of 1000 m of altitude generally outlines the border between the coastal plain (in greenish shades) and the mountain range, and the plateau to the west (red shades).

Some major cities in the region – São Francisco do Sul, Florianópolis, Laguna, and Araranguá – are indicated, as well as the location of LiDAR measuring points: the first one on the UFSC Campus in the city of Araranguá, and the second one at the Ocean and Atmosphere Observation Base (BOOA) in Balneário Arroio do Silva.

The longitudinal topographic-bathymetric transects to the north, center, and south of the domain are shown in Figure 1b. The mountain range (> 800 m), coastal plain (0 to 200 m), and continental shelf (-200 to 0 m) can be identified in the figure. In the central transect, the Santa Catarina Island is characterized by a low relief at -48.5 W.

2.2 Atmospheric Modeling

The atmospheric modeling results used in this work come from the SeaWind-StaCatarina database developed by the Environmental Hydraulics Institute from the University of Cantabria, Spain. This product was obtained through a dynamic downscaling of the WRF model (3.5 version) and of the Advanced Research WRF (ARW) dynamics solver developed by the National Center for Atmospheric Research (NCAR).

The CFSR reanalysis (Saha et al., 2010) was used as an input and to prescribe the boundary conditions of the WRF model. The simulated period covered 32 years, from 1979 to 2010. The simulation was performed through two successive nestings in grids of 9 and 3 km of resolution. The SeaWind-StaCatarina results were validated against seven conventional meteorological stations, one of them located offshore at 78 m high (Menendez et al., 2011). According to the report from the CEPAL project (2015), the Root Mean Square Error (RMSE), the bias, and the R^2 between the offshore station and the modeling results were equal to 2.83, 0.65, and 0.59, respectively. The u and v components of the wind were available in hourly averages at five heights: 10, 50, 90, 120, and 150 m above the land (or sea) surface. The air temperature at 2 m high and atmospheric pressure at sea level were also available. For the calculations of turbine production, the wind speed $U=\sqrt{u^2 + v^2}$ at 90 m high was used. Details of the model configuration are described in Menendez et al. (2011; 2014) and Fernandez-Quiruelas et al. (2015). Salvação et al. (2014) performed wind simulations using the WRF and the Penn State–NCAR fifth-generation Mesoscale (MM5)

models and compared their results with instrumentation data. They concluded that the WRF model faithfully represents the wind in both coastal and open ocean regions.

2.3 LiDAR Profiler

The wind vertical profiles were measured by a LiDAR (Light Detection and Ranging), equipment that works with an infrared laser technology for remote sensing of the atmosphere. The equipment used was the Zephir ZP300, which performs up to 10 measurements of wind direction and intensity between 0 and 200 m high (Nassif et al., 2018). Measurements are performed sequentially, taking approximately 15 seconds to complete each vertical profile.

Two observation bases were constructed to measure the coastal winds. The first one was located on the urban area of UFSC Campus in Araranguá, SC, near 9 km from the coast (Figure 2a). The second one was located on the Entremares Fishing Platform in Balneário Arroio do Silva, SC, approximately 250 m away from the beach line (Figure 2b). In both locations, it was necessary to build a concrete base and an electricity connection with uninterruptible power supply (UPS) for the LiDAR operation. On the fishing platform, a laboratory called Ocean and Atmosphere Observation Base (BOOA[4]) was built, where a meteorological tower was additionally installed (Figure 2b). The LiDAR profiler was installed at the top of BOOA, about 10 m higher than the mean sea level. The time series from the UFSC campus covered the period from April to December 2016, while the data from BOOA was

---

[4] Base de Observação do Oceano e Atmosfera (BOOA)

recorded from December, 2016 to December, 2017. The LiDAR profiler was removed from the fixed stations from September 19 to 22, 2017, and from November 5 to 26, same year, to perform boat measurements, which will be considered in future communications. Considering the periods of fixed measurements analyzed in this article, the data losses were minimal and only about 0.35% of the data were considered invalid. In the BOOA, the winds were measured at the heights of 20, 30, 50, 90, 110, 150, 170, 190, and 210 m above mean sea level; on the other hand, the observations on the UFSC Campus corresponded to 11, 21, 40, 60, 80, 100, 140, 160, 180, and 200 m above ground level.

2.4 Power density

The power density, P_d (Wm^{-2}), represents the kinetic energy flux per unit area, which is a function of the air density, ρ (kgm^{-3}), and of the cube of the wind speed, U (ms^{-1}). P_d can be calculated for a time series of N observations through the equation:

$$P_d = \frac{1}{2N} \sum_{i=1}^{N} \rho_i U_i^3 \text{ (Equation 1)}$$

Where the index i represents each WRF measurement. The actual production expected from a turbine depends on the rotor area and on the efficiencies of the mechanical and electrical systems. However, the power density is useful for estimations since it is independent of the turbine characteristics.

Altitude and air temperature influence the air density and consequently P_d. To calculate the air density, the pressure at sea level P_o (Nm^{-2}) was converted to pressure at altitude:

$$P = P_o \exp(-z/H) \text{ (Equation 2)}$$

Where P_o is given by the model and $H = RT/g$ refers to the scale height, where T is the air temperature, g is the acceleration of gravity, and $R = 287 \text{ J K}^{-1} \text{ Kg}^{-1}$ is the dry air constant[5] (Wallace and Hobbs, 2006). The turbine altitude is represented by $z = h + 90$, where h is the topographic altitude of the continental points and 90 m refers to the turbine hub height. In the oceanic region, the same equation is applied by assuming h=0 for the mean sea level. With the calculated pressure P, the air density can be calculated through the equation:

$$\rho = P/(RT) \text{ (Equation 3)}$$

And ρ can be used in Eq. 1 for the power density calculation.

2.5 Wind power production

Three wind turbines used in offshore installations with different sizes were selected for the study: Vestas V90-3 MW, Senvion 152- 6.2M, and Vestas V164-8.0 MW. These horizontal axis turbines consist of three blades and their characteristics are summarized in Table 1.

The generation of power can be calculated through wind speed power curves, $P_i = f(U_i)$, provided by the manufacturers (Figure 3). Turbines begin to produce energy with speeds around 3.5 ms^{-1}, the so-called cut-in speed. After this point, the power increases with the cubed wind speed until the turbine reaches the rated speed, which is when the

---

[4] The SeaWind-StaCatarina database does not supply air humidity, which is necessary for the virtual temperature calculation and use of the general equation for humid air.

maximum capacity is reached. The turbine maintains constant production for wind speeds above the rated speed, but it shuts off if the "cut-out" speed is reached in order to avoid structural damage. The average power of a turbine, Pt (Watts), can be calculated for each point of a numerical grid using the wind speed, U_i, and the power curves, $P_i=f(U_i)$:

$$P_T = \frac{1}{N}\sum_{i=1}^{N} f(U_i) \text{ (Equation 4)}$$

Once the power generated at each grid point is estimated, the wind resource can be spatially integrated for specific geographic regions:

$$P_R = \sum_{j=1}^{M} P_{Tj} D A_j \text{ (Equation 5)}$$

Where j spatially identifies the considered grid point and M represents the total number of points of the selected continental or oceanic area. D refers to turbine density per km². It is taken into account that each turbine occupies a surface area of 7 d x 10 d, where d is the diameter of the turbines (Manwell et al., 2009). Considering d=152 for the Senvion 6.2 turbine, this corresponds to D=0.62 turbines per km² (Table 1).

3. Results

3.1 Seasonal Fields

Wind speed

The climatological seasonal wind fields are shown in Figure 4. The colors on the map represent the wind speed (ms⁻¹) at the height of 90 m

above the surface. The bathymetric contours of 30, 50, and 100 m are outlined as well as the topographic contour of 1,000 m of altitude.

A strong influence of the South Atlantic High is observed during the summer and spring (Figures 4a, d), when winds predominantly blow from the northeast. On the other hand, in the fall and winter (Fig. 4b, c), the westerlies become notably more important (Cavalcanti et al., 2009; Pimenta et al., 2018).

In general, significant speed gradients were observed between the coastal plain and the adjacent oceanic region, with differences varying from 2 to 5 ms^{-1} at 90 m high. In the oceanic region, speeds increase towards the south of the state. Typical differences of 2 up to 4 ms^{-1} can be observed in the winter and spring between the latitudes of 26 and 29°S around the 50 m deep isobath (Fig. 4c, d).

In the summer and fall, the south of the state presented average winds of the order of 8 to 9 ms^{-1}. In the austral winter and spring, those averages reached 9 ms^{-1} and 10 ms^{-1}, respectively, off Araranguá at the latitude of 29°S. In the SC mountain range, the average speeds were also significant and much higher than the observed winds on the coastal plain. The intensity values observed along the mountain range at the altitude of 1,000 m were comparable in magnitude to the offshore winds (Figure 4c).

Pimenta et al. (2008) studied the average speed at 80 m high using QuikSCAT satellite data in the period from 1999 to 2007, indicating intensities of 9 ms^{-1} in the oceanic region, decreasing to 7.8 ms^{-1} north of SC. The average offshore wind speed (Table 1) was within the operating range of modern turbines (3 to 20 ms^{-1}) and very close to the nominal speed (between 12 and 14 ms^{-1}).

South from Laguna, between 28.5 and 29$^{°}$ S, it was possible to observe a region of coastal "shading", with strong cross-shore speed gradients. The region of lower wind velocities occurred in a curved portion of the shoreline. This decrease in wind intensity can be a result of the frictional effects and topography elements from Santa Marta Cape region (to the north) over the prevailing northeastern winds.

Power density

Climatological maps of power density seasonal averages are shown in Figure 5. These fields were calculated through Equations 1 and 3 and facilitate the identification of the most promising sites for the implementations of wind farms.

In the southern region of the state, near Santa Marta Cape, the highest power densities are observed in shallow regions (> 20 m deep), ranging from 550 to 700 Wm^{-2}. When considering deeper regions (20 to 100 m deep), significant resources (> 700 Wm^{-2}) were also found south of Santa Marta Cape. The maximum offshore average power density (920 Wm^{-2}) occurred in the spring around the depth of 50 m, at the latitude of 28.75°S and longitude of 49.1°W (Figure 5d). In the continental region, the mountainous area between 27.75°S and 29°S presented values over 1,000 Wm^{-2}.

The seasonal latitudinal variation is notable and larger resources (over 500 Wm^{-2}) are found below the latitude of 28°S, in the south of the state. Manwell (2009) suggested that values of 400 Wm^{-2} are considered good, and values over 700 Wm^{-2} are optimal for wind generation. Pimenta et al. (2008) evaluated the power density at 80 m high and found values of 750 Wm^{-2}, 550 Wm^{-2}, and 450 Wm^{-2} in the southern,

central and northern region of the state, respectively, already demonstrating a significant difference in potentials between north and south of the state. Silva et al. (2015) studied the seasonal variation of power densities in the Brazilian coast using satellite data. For the SC state, the densities were between 450-600 Wm^{-2} in the summer, 750 Wm^{-2} in the fall, and between 600-900 Wm^{-2} in the winter and spring. Carvalho et al. (2017) mapped the power density on the coasts of Portugal and Spain, reaching up to 500 Wm^{-2} in the region of Galicia.

The South Atlantic High Pressure has dominant influence over surface winds in southern Brazil. The system is present in the region during all seasons, but is stronger in the winter. Seasonal movements of this high-pressure system determine the strength of penetration of low-level winds along the coast (Silva et al., 2015; Cavalcanti et al., 2009). Polar air masses associated with cold fronts frequently reach this area throughout the year and are more intense between the fall and winter.

Production of turbines

Figures 6 and 7 show the maps of average turbine power calculated through Equation 4 and the power curves of Vestas (VE) turbines of 3 and 8 MW of capacity, respectively. These results highlight the characteristics that were previously described – strong cross-shore gradients between the coastal and oceanic regions, besides the large latitudinal variation (north-south).

Low production is observed over the coastal plains, with values lower than 600 kW and 1,000 kW for the 3-MW and 8-MW VE, respectively, corresponding to a capacity factor (CF) between 10 and 20%. On the other hand, in the oceanic region south of 27.5°S, the production

reached an average of 1.7 MW (CF=56%) and a value of 3.7 MW (CF=46%) considering the 3-MW and 8-MW VE, respectively.

The technical potential of resources was calculated through Equation 5 considering different wind turbines and was organized according to topographic/bathymetric limits, presented in Table 2. The table not only indicates the area available for the installation of turbines, As (km^2), but also the potential resource, P_R (GW), and the resource density calculated by the ratio between potential and area, P_R/A_S (MW km^{-2}).

The best performance corresponded to the 3-MW VE turbine, followed by the 6.2-MW Senvion. The offshore resource potential between 0 and 20 m deep was around 9 GW, increasing to 39 GW for the interval between 0 and 50 m deep. The oceanic resource potential between 0 and 1,000 m deep was equal to 192 GW, but dependent on a diversified used of foundations, including flotation technologies. The continental resource potential between 0 and 1,000 m high was smaller and reached 93 GW, also showing a lower resource density of 1.71 MW km^{-2} when compared to the oceanic region, where the average was 3.22 MW km^{-2}.

3.2 Cross-shore vertical transects

Figure 8 explores the cross-shore structure of winds for the three transects identified in Figure 1. The North sector (N) is located off São Francisco do Sul, the Central sector (C) is off Florianópolis, and the South sector (S) is at Araranguá latitude. Colors represent the WRF climatological wind speed averages (1979-2010) for the austral spring (Sep-Oct-Nov). The left panels illustrate the vertical distribution of winds in scale with the topographic and bathymetric variations. The modeling results covered the lower atmospheric boundary layer,

between 0 and 150 m above the surface. The figures clearly show an intensification of winds from north to south and the drastic wind deceleration over the coastal plain, between 0 and 100 m of altitude. The wind acceleration in the summit of the Serra do Mar mountain range is also evident.

The right panels show the lower atmospheric boundary layer in more detail, between 0 and 150 m high above the land (or sea) surface. A vertical dotted line represents the position of the coastline. In the three transects, it is possible to identify a "coastal boundary layer", or transition region of continental winds (below 4 ms^{-1}) to most intense winds of the oceanic region (> 6 ms^{-1}). The region of orographic wind intensification around 50°W in the south sector and 49°W in the central and northern transects. The largest vertical shear in the oceanic region is found near the coast and in the central transect.

Since the majority of current modern wind turbines are between 90 and 100 m high, the most significant wind intensities for exploration (> 8 ms^{-1}) were located in the south section, east of 49°W. This section suggest the presence of a low-level atmospheric jet around 48.5°W with wind intensities above 10 ms^{-1}. Soares et al. (2014) found jets in the Iberian Peninsula between 300-400 m of altitude with average speeds of 15 ms^{-1} and maximum speeds of 25 ms^{-1}.

3.3 Mean vertical profiles

Time series were used to calculate the vertical profiles of average wind speed (Figure 9). Fourteen grid points were selected from the model for the previously defined North (N), Central (C), and South (S) transects (Figure 1). Each sector compares different points between the continental and oceanic regions. The red line represents profiles in the mountainous region at 1,000 m of altitude (LAND); the black line identifies coastal points near the coastline (COAST); blue lines represent oceanic points near the 30- and 50-m isobaths (OCEAN). In the central panel, there is a vertical profile measured on the Bay of Florianópolis (BAY, green line). In the S sector, points from the model were also selected near the Ocean and Atmosphere Observation Base (BOOA) and over the UFSC Campus in Araranguá. Figure 9c identifies the data measured by the LiDAR profiler in those two stations.

The northern region of the state of SC is the only location where the offshore winds were lower than 7 ms^{-1} at 100 m high (Figure 9a). Surprisingly, mountain winds were slightly higher than the offshore winds at this latitude, highlighting the importance of topographic effects on wind intensification. In this transect, it is clear that the vertical shear in coastal sites is larger than in the oceanic sites.

Offshore winds above 100 m from the surface gained intensity towards the south, reaching 7.6 ms^{-1} in the C sector and 8.5 ms^{-1} in the S sector at 50 m deep. In the central transect, the orographic effect on the wind acceleration was not significant; the mountain winds were lower than 4 ms^{-1}. Winds over the Bay of Florianopolis were also less intense than those winds in the coastal region – at the exposed oceanic side of the Santa Catarina Island (Figure 9b).

In the S sector, topographic effects can significantly accelerate the winds in the mountainous region (Figure 9c). The wind speeds at 100 m high in the mountain vertical profile (LAND) were comparable to the velocities from the oceanic profile at 30 m deep (OCEAN), even although they experienced a vertical shear almost three times larger. Winds from the coastal plain (UFSC) 9 km off the coast had lower intensities than those coastal winds near the coast (BOOA), suggesting that the roughness effects of the terrain are significant in defining a coastal boundary layer.

In the S sector, the highest average speeds occurred in all vertical profiles. Not only do offshore winds intensify towards the south of the state, but also the coastal and mountain winds (Figure 9c).

LiDAR measurements at the BOOA site led to an average wind speed of 6.1 ms^{-1} at 100 m high, while the WRF model resulted in an average intensity of 6.6 ms^{-1} (Figure 9c). This comparison, however, should be carefully considered since the model vertical profile represents a climatological profile (1979-2010), while the LiDAR data corresponds to a one-year period (2017). Although the model overestimated the LiDAR wind speeds in 0.5 ms^{-1}, we associate this difference to interannual variability. Previous comparisons made by CEPAL (2015) with paired data have shown that the winds from the Sea Wind Sta-Catarina database are well correlated with observations from meteorological buoys. Similar differences are found in the comparison between the model climatological vertical profile and the measurements at the UFSC site; LiDAR observations were equal to 4.5 ms^{-1} at 100 m high, while the model provided a value of 5 ms^{-1}. In this situation, the period of LiDAR measurements was from April to December 2016.

Although the measurement periods were different, vertical profiles observed in both locations showed a vertical shear that was comparable to that described by the model.

Together, these results highlight the importance of the terrain in the determination of vertical profiles. In mountainous regions, orographic effects can accelerate winds, but under intense vertical shear. In coastal regions, the effect of terrain roughness was fundamental. Winds tend to blow in directions close to the orientation of the coastline in this region. Thus, the interaction with the rough terrain can lead to the development of the inner boundary layer (Arya, 2001). Even near the coast, the effect of friction from the soil significantly influenced the wind speed at 100 m of altitude. For this reason, oceanic winds were consistently more intense and less sheared than the continental winds.

3.4 Winds at the Ocean and Atmosphere Observation Base (BOOA)

In this section, the model results are explored together with the LiDAR measurements in the coastal observation site of the Ocean and Atmosphere Observation Base (BOOA). For the model, the speed at 90 m high from a grid point located on the ocean near the coordinates of the BOOA was used. The LiDAR data referred to the altitude of 89 m above mean sea level.

Monthly speed variability

Figure 10 shows the monthly distributions of wind speed in the form of boxplots for the BOOA site, comparing the LIDAR data (panel a) with the WRF model results (panel b). These charts identify where the most likely values for each month are located.

The central point on each bar is the median. The edges of the bar are the first (Q1) and third quartiles (Q3), which delimit 50% of the observations. The horizontal lines that extend from the edges of the box are up to 1.5 times the interquartile amplitude (IAQ) [6]. Points outside of the horizontal lines are considered outliers. Table 3 complements the information showed in Figure 10, presenting the median and the percentiles of LiDAR measurements and model results.

During the 12 months, there is great similarity in the wind behavior observed in 2017 in the LiDAR data and in the model climatology. LiDAR mean values ranged from 4.5 to 7.0 ms^{-1}, while the WRF climatology for the same site varied from 4.8 to 7.1 ms^{-1}. Monthly analyzing the WRF model climatology, it showed higher values than the LiDAR data for all months, except for August.

In general, average winds tended to intensify from mid-winter (July) to spring (November). Extreme values above the upper horizontal line occurred in every month. Values above 25 ms^{-1} were only observed in June in the LiDAR data.

---

[6] The interquartile height refers to the height of the bar AIQ = Q$_3$-Q$_1$. Lower horizontal line limit: (Q$_1$ - 1.5 AIQ); upper horizontal line limit: (Q$_3$ + 1.5 AIQ).

Directional speed histograms

Figure 11 compares the directional speed histograms of the WRF model (left) with the ones of the LiDAR data for the BOOA site. The analyzed months referred to the summer (Dec-Jan-Feb), fall (Mar-Apr-May), winter (Jun-Jul-Aug) and spring (Sep-Oct-Nov).

Prevailing northeastern winds represent the role of the South Atlantic High in all seasons. The highest occurrence of the northeastern quadrant occurred in spring (> 45%) and summer, although under higher intensity in the spring, with winds above 14 ms^{-1}. The passage of cyclones and cold fronts is responsible for intense southern winds, which become more important during the winter. Surprisingly, the northeastern winds were dominant during all seasons. Southeastern and northwestern wind conditions were rare and suggest that the wind rotates fast during the passage of cyclones and cold fronts.

Directional distribution of power density

The directional distribution of power density was calculated based on the WRF model climatology and through the LiDAR data (Figure 12). In this analysis, the power density is calculated through the wind time series and then the directional mean is calculated for intervals of 10°. Results are shown in the form of a polar graph, where the radius represents the power density (Wm^{-2}) and the lines represent the seasons. In general, the LiDAR measurements yielded average power density values > 1,000 Wm^{-2} in the northeastern quadrant in spring, of the order of 800 Wm^{-2} for the southwestern quadrant, and very low values (<100 Wm^{-2}) for the continental (northwest) and oceanic (southeast) directions. Periods of higher power density were associated with the spring and fall.

Model results show similar distributions, but with smoother patterns. Maximum density powers in the northeastern direction occurred in the spring (1000 Wm^{-2}) and summer (750 Wm^{-2}). For the southwestern quadrant, the most intense winds took place in the spring and autumn (> 500 Wm^{-2}).

4. Discussion

Results show that the southern region of the state of Santa Catarina had the highest available wind potential. Resource significantly increases in the oceanic region and away from the coast. Good agreement was found comparing WRF model results with LiDAR data. The region with the highest productivity is located south of Laguna, and the energy resources are very expressive up to 100 m deep. At the height of current turbines (100 m), average speeds of 8.5 ms^{-1} were observed over the 50 m isobath.

Average wind production with the 3-MW VE turbine was lower than 600 kW in the coastal plain region. Considering the 8-MW VE turbine, there was a production of 1,000 kW in the same region, providing a capacity factor between 10 and 20%. On the other hand, in the offshore region south of the state, the average production was 1.7 MW and 3.7 MW with the 3- and 8-MW VE turbines, yielding capacity factors of 56% and 46%, respectively. Brazil has an average capacity of 50% for wind generation in the spring against 20-25% for the world average, as published by the Brazilian Wind Energy Association (ABEEolica, 2017). By using LiDAR measurements from the Ocean and Atmosphere Observation Base (BOOA) from May 2017, Nassif et al. (2018) reported

an average production of 2.5 MW with the 8-MW VE turbine, providing a capacity factor of 32%, which was the highest of the evaluated months.

Weiss et al. (2018) evaluated the spatial planning of the southern Brazilian coastal region for the implementation of onshore wind farms and pointed out that the impacts on biota were evident, especially in the study area due to its environmental diversity. Therefore, environmental studies and diagnostics will be essential to assess impacts during the installation of wind farms when there is a high circulation of vessels and high noise generation due to the installation of foundations, consequently damaging the marine substrate. Regarding the operation stage of a wind farm, the impacts are probably minimized. There are studies that have reported minimal interference of wind farms in migration routes (Dierschke et al., 2006); others that have suggested the creation of artificial reefs due to the presence of turbine foundations (Inger et al., 2009; Salcedo-Sanz et al., 2014) and the co-production with aquaculture of species such as fish or crustaceans (Griffin et al., 2015). It is still uncertain whether the degree of impact of offshore wind farms is comparable, higher or lower than that of onshore wind farms. Most likely, the impact levels will be dependent on the local diversity of the considered continental and oceanic regions.

The South Atlantic Convergence Zone (SACZ), the South Atlantic Subtropical Anticyclone, cold fronts, jet streams, and passage of cyclones are the main climatic factors affecting the winds in the southern region of Brazil. Pes et al. (2017) analyzed extreme winds assessing climate change trends, pointing out that in the southern and southeastern region of Brazil, there is a tendency of decreasing the

frequency of extreme winds above 25 ms^{-1}. On the other hand, the authors suggested an increase in average speeds, which would improve the wind energy production without affecting the structure of the wind turbines.

The area with the greatest wind potential for the implementation of an offshore farm was located outside the Baleia Franca Environmental Preservation Area (EPA), a protected area between the cities of Florianópolis and Balneário Rincão, covering nine municipalities, an area of 156.000 hectares, and 130 km of coastline. However, the southern region is on the migration route of marine mammals, also subject to intense harbor and fishing activity. A detailed study on the impacts on wildlife and economic activities is necessary. Wind facilities at depths greater than 50 m were studied by Koh et al. (2016), concluding that fixed structures at great depths would be very expensive, suggesting that floating technologies were the best option. In his study, four floating models were presented, whose prototypes are in test stages.

Emphasis should be placed on the need for greater knowledge on turbine foundation issues, optimization of electrical connections, and stages of offshore construction and operation. The wind in southern regions represents a new market for Brazilian investors who are initiating negotiations on this renewable source by considering its potential for extraction.

5. Summary and Conclusions

This work evaluated the coastal and offshore wind potential of the state of Santa Catarina, comparing the northern, central, and southern regions. A 32-year time series of wind data at five heights was used in WRF modeling. The evaluation of LiDAR profiler data installed at a urban and a coastal location was also performed.

Although it has a narrow continental shelf, the Santa Catarina state has a significant potential for development of offshore wind energy. The region with the greatest potential and viability for a wind farm implementation was offshore, near the city of Araranguá.

It was verified that the northern region of the state showed the lowest power density at 90 m high, while the southern region yielded the best potential. The turbine that resulted in greater potentials for the simulated region was the 3-MW Vestas. The exploration could be developed today by using the existing and widespread monopile turbine technology. With the new floating facilities being tested, exploration will be even more viable.

The installation of an offshore wind farm could leverage greater efforts if marine hydrodynamics technologies (wave energy, tide, and currents) were considered, but they have been poorly developed so far in Brazil. The optimal situation would be if those technologies reached maturity similar to that of onshore wind energy and took part in the Brazilian electricity market in the near future.

ACKNOWLEDGMENTS

REFERENCES

Amante, C. and B.W. Eakins. ETOPO1 1 Arc-Minute Global Relief Model: Procedures, Data Sources and Analysis. NOAA Technical Memorandum NESDIS NGDC-24. National Geophysical Data Center, NOAA. doi:10.7289/V5C8276M [Accessed: March 2017] ,2009.

Amarante O. A. Camargo do; Zack J., Brower M.; Sá A. Leite. Atlas of Brazilian Wind Potential. Brasília, Brasil, Centro de Pesquisas de Energia Elétrica (Cepel). In Portuguese. 2001.

ANEEL. Generation Information Bank: Generation Capacity of Brazil. In Portuguese. Available in: <http://www2.aneel.gov.br>. Access em: 10 de Abril de 2018. 2017

Archer, C. L., AND M. Z. JACOBSON, Evaluation of global wind power, *J. Geophys. Res.*, 110, D12110, doi:10.1029/2004JD005462, 2005.

Archer, C. L., and Coauthors: Meteorology for coastal/offshore wind energy in the United States: Recommendations and research needs for the next 10 years. Bull. American Meteorological Society, 95, 515–519, 2014.

Arya, Paul S. Introduction to micrometeorology. Vol. 79. Elsevier, 2001.

Boyle, Godfrey (2004). Renewable Energy. Power for a Sustainable Future. Oxford. 452 pp.

Capps, S. B.; Zender, C. S. Global ocean Wind power sensitivity to surface of layer stability. Geophysical Research Letters, Wiley Online Library, v. 36, n. 9, 2009.

Carvalho, D. et al. Offshore winds and wind energy production estimates derived from ASCAT, OSCAT, numerical weather prediction models and buoys−A comparative study for the Iberian Peninsula Atlantic coast. Renewable Energy, v. 102, p. 433-444. 2017.

Cavalcanti, Iracema F. de Albuquerque; FERREIRA, Nelson Jesus; SILVA, Maria Gertrudes A. Justi; DIAS, Maria A. F. da Silva. Tempo e Clima no Brasil. In Portuguese. Oficina e Textos. ISBN 978-85-86238-92-5, São Paulo, 528p, 2009.

Charlier e Justus. Ocean Energies: Environmental, Economic and Technological Aspects of Alternative Power Sources. Elsevier Oceanography Series. 534 pp. 1990.

CEPAL. Generation and Integration of historical climate databases and projections of climate change for coastal risk management in the state of Santa Catarina, Brazil. In Spanish. Economic Commission for Latin America and the Caribbean, 2015.

Dierschke, V., Garthe, S.,Mendel,B. Possible Conflicts between Offshore Wind Farms and Seabirds in the German Sectors of North Sea and Baltic Sea. [KÖLLER, Julia; KÖPPEL, Johann; PETERS,

Wolfgang (Ed.)]. Offshore wind energy: research on environmental impacts. Springer Science & Business Media, 368 pg, 2006.

Dvorak MJ, Archer CL, Jacobson MZ. California offshore wind energy potential. Renewable Energy 2010;35:1244e54. http://dx.doi.org/10.1016/ j.renene.2009.11.022. 2010.

Dvorak, M. J., Corcoran, B. A., Ten Hoeve, J. E., McIntyre, N. G. and Jacobson, M., US East Coast offshore wind energy resources and their relationship to peak-time electricity demand. Wind Energy, 16: 977-997. doi:10.1002/we.1524. 2013.

FAPESP. Brazil's onshore wind potential may be six times higher than estimated. October 2016. In Portuguese. Agency FAPESP. <http://agencia.fapesp.br/>. Accessed in 01/02/2018.

Fernández Quiruelas, V., Fernández Fernández, J., Cofiño González, A. S., Blanco Real, J. C., García Díez, M., Magariño Manero, M. E., ... & Gutiérrez Llorente, J. M. WRF4G: WRF experiment management made simple. 2015.

Garvine, Richard W.; Kempton, Willett. Assessing the wind field over the continental shelf as a resource for electric power. Journal of Marine Research, v. 66, n. 6, p. 751-773, 2008.

Global Wind Energy Council (GWEC)- Global Wind Report- Annual Market Update. 2017

Griffin, Robert, Bela Buck, and Gesche Krause. "Private incentives for the emergence of co-production of offshore wind energy and mussel aquaculture." Aquaculture 436 (2015): 80-89. 2015P

Hasager CB, Barthelmie RJ, Christiansen MB, Nielsen M, Pryor SC. Quantifying offshore wind resources from satellite wind maps: study area the North Sea. Wind Energy;9:63–74. 2006a.

Hasager CB, Nielsen PA, Astrup P, Barthelmie ED, Dellwik E, et al. Offshore wind resource estimation from satellite SAR wind field maps. Wind Energy. 8:403–19. 2006b.

HYWIND. Hywind Scotland Pilot Park, Tech. rep. 2016. <http://www.statoil.com>. Accessed in 10/08/2017.

Inger, R., Attrill, M. J., Bearhop, S., Broderick, A. C., James Grecian, W., Hodgson, D. J.,… & Godley, B. J. Marine renewable energy: potential benefits to biodiversity? An urgent call for research. Journal of Applied Ecology, 46(6), 1145-1153. 2009.

IPCC- Intergovernmental Panel on Climate Change, Special Report on Renewable Energy Sources and Climate Change Mitigation: Summary for Policymakers and Technical Summary, Intergovernmental Panel on Climate change, Geneva, 2011.

Jacobson, M. Z., Delucchi, M. A., Bauer, Z. A., Goodman, S. C., Chapman, W. E., Cameron, M. A., ... & Erwin, J. R. 100% clean and renewable wind, water, and sunlight all-sector energy roadmaps for 139 countries of the world. Joule, 1(1), 108-121.2017.

Kempton, Willett et al. Electric power from offshore wind via synoptic-scale interconnection. Proceedings of the National Academy of Sciences, v. 107, n. 16, p. 7240-7245, 2010.

Koh, J. H.; NG, E. Y. K. Downwind offshore wind turbines: Opportunities, trends and technical challenges. Renewable and Sustainable Energy Reviews, v. 54, p. 797-808, 2016

Li Ji-Hang, Guo Zhen-Hai & Wang Hui-Jun. Analysis of Wind Power Assessment Based on the WRF Model, Atmospheric and Oceanic Science Letters, 7:2, 126-131, 2014.

Liu, W. Timothy; TANG, Wenqing; XIE, Xiaosu. Wind power distribution over the ocean. Geophysical Research Letters, v. 35, n. 13, 2008.

Lu, X., McElroy M. B. and Kiviluoma J. Global potential for wind-generated electricity. Proceedings of the National Academy of Sciences, 106 (27) 10933-10938. DOI: 10.1073/pnas.0904101106, 2009.

Manwell, J. F.; Mcgowan, J. G.; Rogers, A. L. Wind Energy Explained: Theory, Design and Application. 2a Edition. ed. Massachusetts: John Wiley & Sons, 705 p., 2009.

Mattar, C., & Guzmán-Ibarra, M. C. A techno-economic assessment of offshore wind energy in Chile. Energy, 133, 191-205. 2017a.

Mattar, C. & Guzmán-Ibarra, M. C. Offshore wind power simulation by using WRF in the central coast of Chile. Renewable Energy, 94, 22-31.doi.org/10.1016/j.renene.2016.03.005. 2017b.

Menendez M, Tomas A, Camus P, Garcia-Diez M, Fita L, Fernandez J, et al. A methodology to evaluate regional-scale offshore wind energy resources. Ocean 2011 IEEE Spain 2011:1e8. doi:10.1109/Oceans-Spain.2011.6003595.

Menendez, M. et al. High-resolution sea wind hindcasts over the Mediterranean area. Climate dynamics, v. 42, n. 7-8, p. 1857-1872, 2014.

Monaldo FM, Thompson DR, Pichel WG, Clemente-Colon P. A systematic comparison of QuikSCAT and SAR ocean surface speeds. IEEE Trans Geosci Remote Sensing 2004;42:283–91.

Nassif F. B., Pimenta F. M., D'Aquino C. A., Assireu A. T., Passos J. Wind profile measurements using a LIDAR over a coastal pier. Submitted to Revista Brasileira de Meteorologia. 2018.

Oliveira, S. S. and Souza, E. P. Analysis of Mesoscale Models for Characterization of the Wind Potential of the State of Paraíba. In Portuguese. Revista Brasileira de Meteorologia, 32(2), 277-291. https://dx.doi.org/10.1590/0102-77863220009. 2017.

Ortiz, G. P.; Kampel, M. Offshore Wind Energy Potential on the Brazilian Margin. In Portuguese. In: V Brazilian Symposium on Oceanography, Santos, SP. 2011.

Pes, M. P., Pereira, E. B., Marengo, J. A., Martins, F. R., Heinemann, D., & Schmidt, M. Climate trends on the extreme winds in Brazil. Renewable Energy, 109, 110-120. 2017.

Pimenta F. M., Kempton, W., & Garvine, R.. Combining meteorological stations and satellite data to evaluate the offshore wind power resource of Southeastern Brazil. Renewable Energy, doi:10.1016/ j.renene.2008.01.012. 2008.

Pimenta F. M., Silva, A. R., Assireu, A. T. Brazil offshore wind resources and atmospheric surface layer stability. Submitt. 2018.

Pryor, S. C.; Barthelmie, R. J. Assessing the vulnerability of wind energy to climate change and extreme events. Climatic change, v. 121, n. 1, p. 79-91, 2013.

Rodrigues, S. et al. Trends of offshore Wind projects. Renewable and Sustainable Energy Reviews, Elsevier, v. 49, p. 1114-1135, 2015.

Saha, S., et al.: The NCEP Climate Forecast System Reanalysis. Bull. Amer. Meteor. Soc., 91, 1015–1058, https://doi.org/10.1175/2010BAMS3001.1. 2010.

Salcedo-sanz, S. et al. Offshore wind farm design with the Coral Reefs Optimization algorithm. Renewable Energy, v. 63, p. 109-115, 2014.

Salvação, N., Bernardino, M., & Soares, C. G. Assessing mesoscale wind simulations in different environments. Computers & Geosciences, 71, 28-36, 2014.

Silva, Allan Rodrigues et al. Complementarity of Brazil′ s hydro and offshore wind power. Renewable and Sustainable Energy Reviews, v. 56, p. 413-427, 2015.

Soares, P. M., Cardoso, R. M., Semedo, Á., Chinita, M. J., & Ranjha, R. Climatology of the Iberia coastal low-level wind jet: weather research forecasting model high-resolution results. Tellus A: Dynamic Meteorology and Oceanography, 66(1), 22377, 2014.

Wallace, John M., and Peter V. Hobbs. Atmospheric science: an introductory survey. Vol. 92. Elsevier, 2006.

Weiss, C. V., Tagliani, P. R. A., Espinoza, J. M. A., de Lima, L. T., & Gandra, T. B. R. Spatial planning for wind farms: perspectives of a coastal area in southern Brazil. *Clean Technologies and Environmental Policy*, 1-12. 2018.

Zhang W. G., J. L. Wilkin, R. J. Chant, Modeling the pathways and mean dynamics of river plume dispersal in the New York Bight, J. Phys. Oceanogr. 1167–1183. doi:10.1175/2008JPO4082.1. 2009.
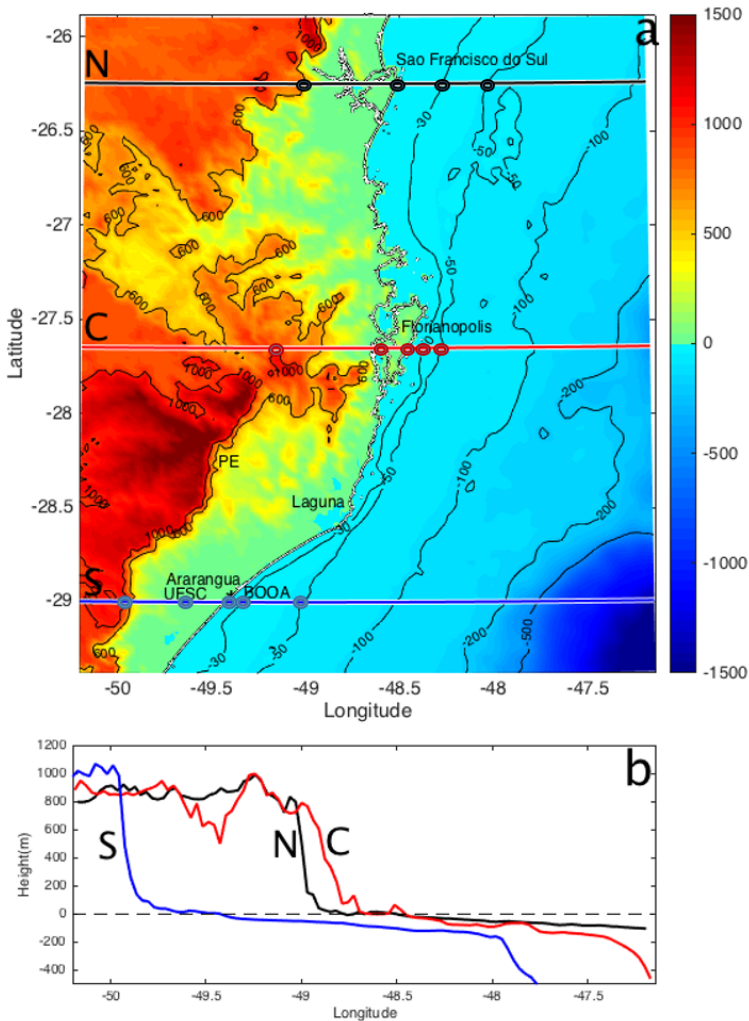
Figure 1 (a) Numerical grid domain of the WRF atmospheric model, including the coastal and offshore region of the state of Santa Catarina (SC) between 26 and 29.5° S. The ETOPO1 digital terrain model is represented by colors. Contours correspond to topography (positive values) and bathymetry (negative values) in meters. The position of the main cities from the state of SC, the UFSC Campus and the Ocean and Atmosphere Observation Base (BOOA) are indicated on the map. **b)** Longitudinal transects of the digital terrain model following the same color set from Fig.1a in order to identify the sectors: South sector (S; blue line), Central sector (C; red line), and North sector (N; black line). The lowest and negative altitudes in the three sectors identify the coastal plain and the continental shelf, respectively. The highest altitudes in the S sector represent the Serra do Mar mountain range.
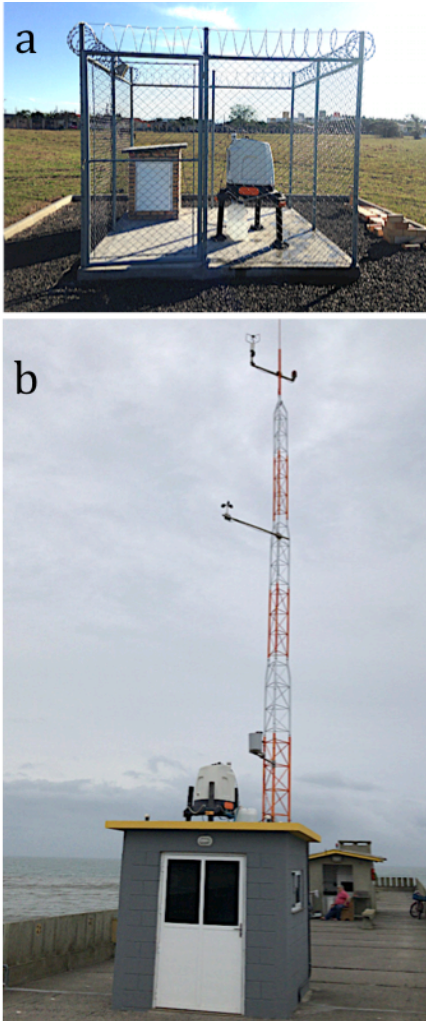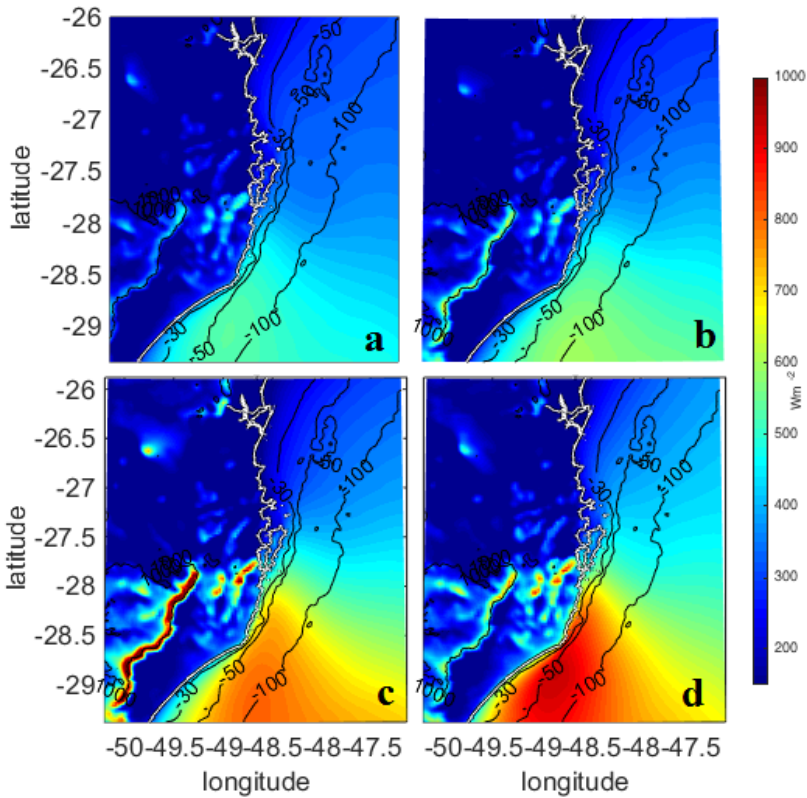
Figure 2 (a) LiDAR base on the UFSC campus in Araranguá, state of SC, Brazil.
(b) Ocean and Atmosphere Observation Base (BOOA) on the Entremares Fishing
Platform in Balneário Arroio Silva, SC, Brazil. Measurement periods were from
June 2016 to December 2016 and from December 2016 to December 2017 on the
UFSC campus in Araranguá and at BOOA, respectively. The LiDAR profiler was
installed at the top of BOOA, around 10 m high from the mean sea level.
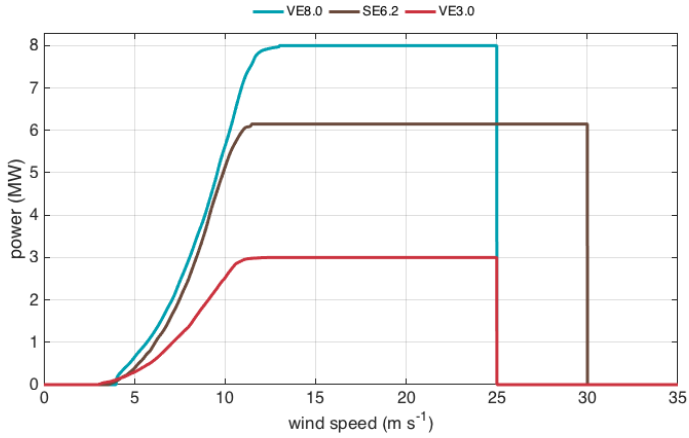
Figure 3 Speed-power curves used applied to the Vestas V90 3 MW (VE3.0; blue line), Senvion 6.2M 152 (SE 6.2; brown line), and Vestas V164-8.0 MW (VE 8.0; red line) turbines.
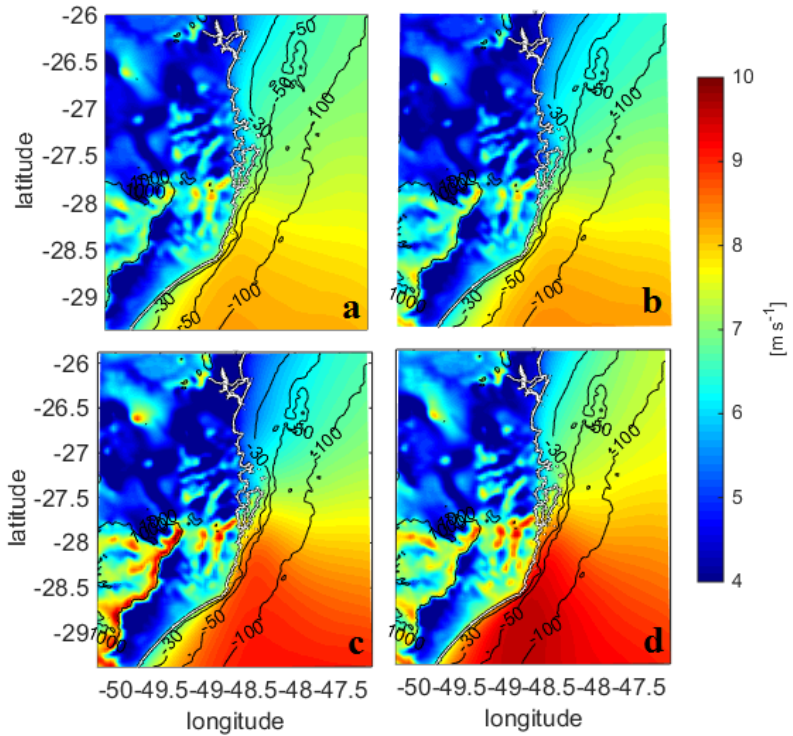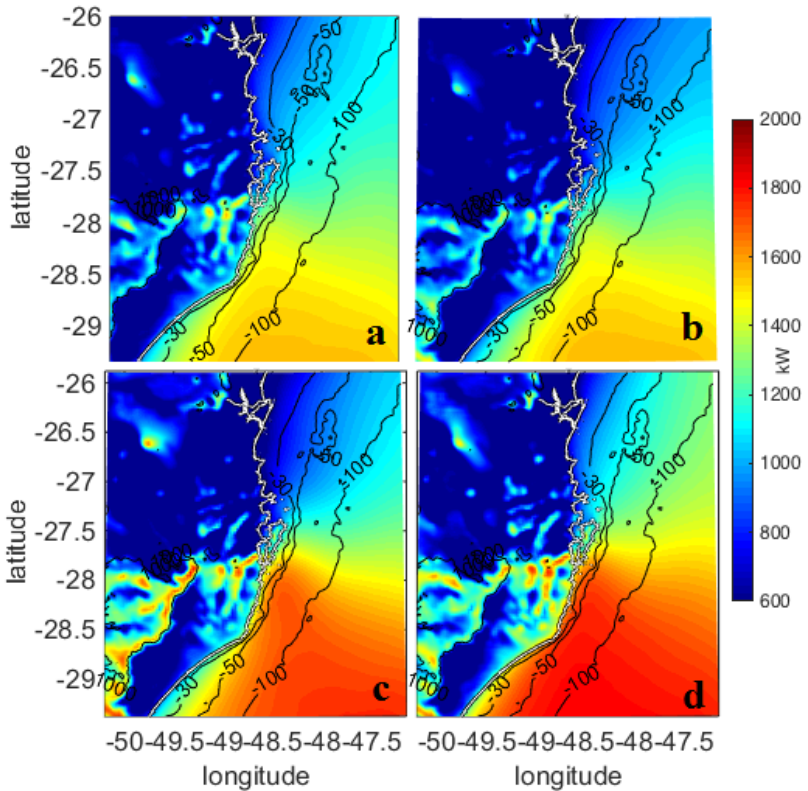
Figure 4 Climatological seasonal fields (1979-2010) of wind intensity at the height of 90 m above the surface. The bathymetric contours of 30, 50, and 100 m are identified. The panels correspond to the **(a)** Summer (Dec-Jan-Feb), **(b)** Fall (Mar-Apr-May), **(c)** Winter (Jun-Jul-Aug), and **(d)** Spring (Sep-Oct-Nov) periods. The color scale represents the wind intensity in ms^{-1}.

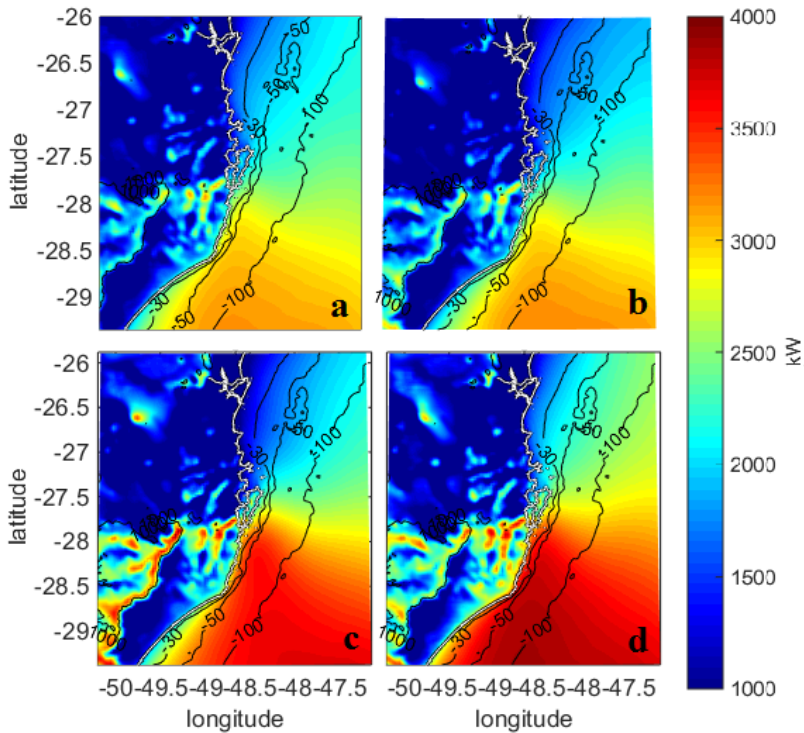**Figure 5** Climatological seasonal fields (1979-2010) of wind power density at the height of 90 m above the surface. The bathymetric contours of 30, 50, and 100 m are identified. The panels correspond to the **(a)** Summer (Dec-Jan-Feb), **(b)** Fall (Mar-Apr-May), **(c)** Winter (Jun-Jul-Aug), and **(d)** Spring (Sep-Oct-Nov) periods. The color scale represents the power density in Wm^{-2}.

Figure 6 Climatological seasonal fields (1979-2010) of practical power generated by a 3-MW Vestas turbine, calculated from winds at the height of 90 m above the surface. The bathymetric contours of 30, 50, and 100 m are identified. The panels correspond to the **(a)** Summer (Dec-Jan-Feb), **(b)** Fall (Mar-Apr-May), **(c)** Winter (Jun-Jul-Aug), and **(d)** Spring (Sep-Oct-Nov) periods. The color scale represents the power in kilowatts (kW).
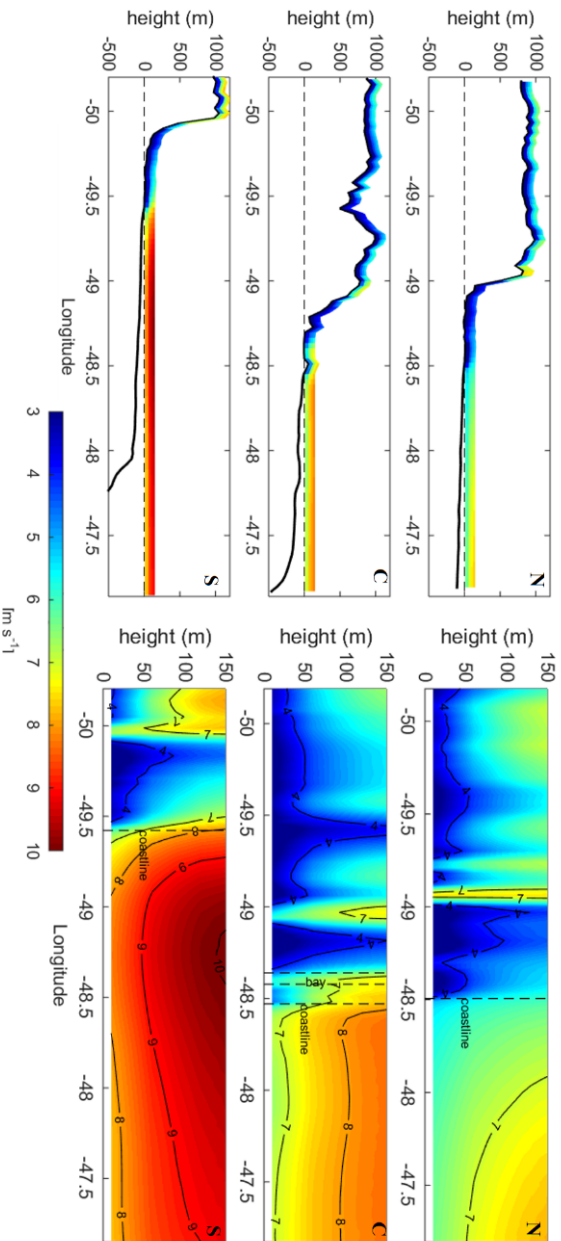
Figure 7 Climatological seasonal fields (1979-2010) of practical power generated by a 8-MW Vestas turbine, calculated from winds at the height of 90 m above the surface. The bathymetric contours of 30, 50, and 100 m are identified. The panels correspond to the **(a)** Summer (Dec-Jan-Feb), **(b)** Fall (Mar-Apr-May), **(c)** Winter (Jun-Jul-Aug), and **(d)** Spring (Sep-Oct-Nov) periods. The color scale indicates the power in kilowatts (kW).
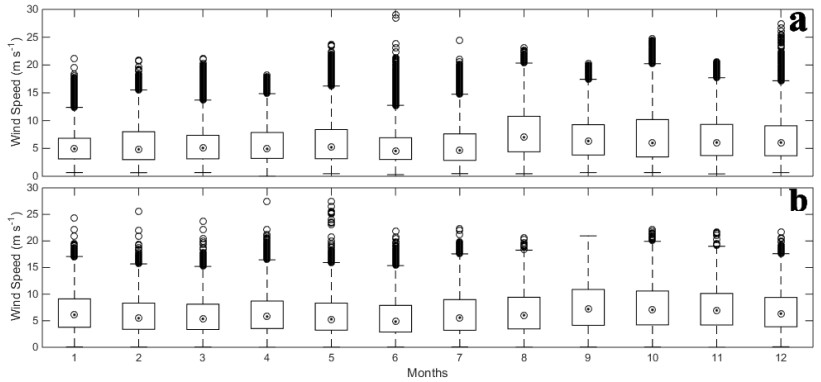
Figure 8 Spring climatological transects of wind intensity as a function of longitude and height. Left panels illustrate the average wind speed in the continental and oceanic regions for the North (N), Central (C) and South (S) sectors. The black continuous contours represent the topography and bathymetry. The panels on the right illustrate the same North (N), Central (C) and South (S) sectors, with detail for the boundary layer between 0 and 150 m high relative to the land (or sea) surface. Vertical dashed lines indicate the coastline and the bay. The position of these sectors is shown in Figure 1a. The color scale represents the wind speed in ms⁻¹.

Figure 9 Mean vertical profiles derived from the modeling results at a 3-km resolution corresponding to the period between 1979-2010. The locations of these vertical profiles are identified in the North (N), Central (C), and South (S) sectors in Figure 1. In the lowest panel, we added LiDAR data from 2017 for comparison.

Figure 10 (a) LiDAR data throughout 2017. **(b)** WRF model results (1979-2010). Monthly variability of wind speed at the BOOA site. Numbers refer to the months of Jan (1), Feb (2), Mar (3), Apr (4), May (5), Jun (6), Jul (7), Aug (8), Sep (9), Oct (10), Nov (11), Dec (12). The central mark in each box is the median; the edges of the box correspond to the 25th and 75th percentiles. The dashes extend to the most extreme data points not considered outliers. Outliers are plotted as circles.

Figure 11 (a) WRF model results (1979-2010) at the BOOA site. **(b)** LiDAR data throughout 2017. Directional wind analysis by season. The percentages represent the number of occurrences in the wind direction and the colors represent the velocities in ms^{-1}.

Figure 12 (a) WRF model results (1979-2010) at the BOOA site. **(b)** LiDAR data throughout 2017. Seasonal analysis of directional power density for the summer (red line; Dec-Jan-Feb), fall (black line; Mar-Apr-May), winter (blue line; Jun-Jul-Aug), and spring (green line; Sep-Oct-Nov). The angles were aligned with the coastline (45°), represented by the thin black line that divides the plot into continental and ocean sectors in green and blue shades, respectively.

Tables

Table 1 Characteristics of three models of modern turbines according to data provided by the manufacturers. Vestas V90-3 MW (VE 3.0), Senvion 6.2M 152 (SE6.2), and Vestas 164-8.0 MW (EV 8.0).

Operation data	Turbine model		
	VE 3.0	SE 6.2	VE 8.0
Rated capacity (kW)	3000	6150	800
Cut-in speed (m s $^{-1}$)	3.5	3.5	4.0
Cut-out speed (m s $^{-1}$)	25	30	25
Rated speed (m s $^{-1}$)	15	11.5	13
Rotor diameter d (m)	90	152	164
Swept area (m^2)	6362	18146	21124
Turbine density D (km^{-2})	1.76	0.62	0.53

Table 2 Practical wind resources based on topographic and bathymetric intervals, and turbine type. In the calculation of the area, exclusion zones such as navigational routes, regions incompatible with the installation of turbines, or areas of environmental preservation were not considered.

	interval	area, A_S	Resource potential, P_R (Resource density=P_R/A_S)		
			VE 3.0	SE 6.2	VE 8.0
LAND	>600 m	27,459 km^2	53 GW (1.94 MW/km^2)	35 GW (1.26 MW/km^2)	31 GW (1.12 MW/km^2)
	0-1,000 m	54,720 km^2	93 GW (1.71 MW/km^2)	60 GW (1.10 MW/km^2)	53 GW (0.98 MW/km^2)
	0-600 m	27,261 km^2	40 GW (1.47 MW/km^2)	26 GW (0.94 MW/km^2)	23 GW (0.83 MW/km^2)
	0-100 m	11,106 km^2	17 GW (1.53 MW/km^2)	11 GW (0.97 MW/km^2)	10 GW (0.86 MW/km^2)
OCEAN	0-20 m	3,870 km^2	9 GW (2.22 MW/km^2)	6 GW (1.46 MW/km^2)	5 GW (1.30 MW/km^2)
	0-30 m	7,002 km^2	16 GW (2.34 MW/km^2)	11 GW (1.54 MW/km^2)	10 GW (1.38 MW/km^2)
	0-50 m	14,976 km^2	39 GW (2.59 MW/km^2)	26 GW (1.72 MW/km^2)	23 GW (1.55 MW/km^2)
	0-100 m	33,714 km^2	99 GW (2.94 MW/km^2)	67 GW (1.97 MW/km^2)	60 GW (1.77 MW/km^2)
	0-500 m	57,663	184 GW	124 GW	111 GW

		km²	(3.19 MW/km²)	(2.15 MW/km²)	(1.93 MW/km²)
	0-1,000 m	59,769 km²	192 GW (3.22 MW/km²)	130 GW (2.17 MW/km²)	117 GW (1.95 MW/km²)

Table 3 Statistical analyzes comparing LIDAR data and model results for each month.

Months	Median		25th Percentile		75th Percentile	
	LIDAR	WRF	LIDAR	WRF	LIDAR	WRF
January	4.94	6.11	3.13	3.78	6.83	9.10
February	4.83	5.47	3.00	3.38	8.01	8.31
March	5.08	5.35	3.14	3.34	7.36	8.11
April	4.92	5.78	3.22	3.53	7.87	8.71
May	5.21	5.27	3.16	3.23	8.38	8.31
June	4.54	4.83	3.03	2.88	6.92	7.88
July	4.66	5.57	2.86	3.21	7.62	8.97
August	7.01	6.03	4.40	3.46	10.78	9.41
September	6.33	7.18	3.83	4.13	9.27	10.89
October	5.99	7.04	3.48	4.22	10.18	10.59
November	6.07	6.94	3.73	4.19	9.32	10.13
December	6.07	6.33	3.70	3.87	9.08	9.38

3 Considerações Finais

Este trabalho avaliou o potencial eólico costeiro e *offshore* do estado de Santa Catarina através de dados de modelagem de mesoescala, gerando mapas de velocidades médias do vento, densidade de potência e geração de energia por diferentes turbinas. Comparamos as regiões norte, centro e sul do estado e a região de maior potencial e viabilidade de implementação de um parque foi na região sul oceânica, próximo a cidade de Araranguá.

Foram analisados 1 ano de dados de vento medidos por um LiDAR, o que permitiu uma comparação com os dados de modelagem, mostrando que o modelo teve uma tendência de superestimar as velocidades de vento. A metodologia utilizada satisfez o propósito do estudo.

Houve uma diferença visível dos recursos entre as áreas analisadas, a região norte apresentou potencial inferior ao da região sul. As maiores velocidades de vento estão ao sul da ilha de Santa Catarina.

Em anexo estão as tabelas 3 e 4 que mostram os resultados de potencial eólico em relação a sazonalidade utilizando a turbina eólica Vestas 3 MW. Os cálculos estão em conformidade com as análises sazonais do capítulo 2. O período de melhor potencial foi a primavera, seguido do inverno, tanto para o continente quanto para o oceano. Os menores valores foram no período de Outono. Na área oceânica, de 7002 km^2, até 30 m, verificou-se potencial de 19 GW na primavera. No Outono e no Inverno o potencial foi de 15 GW. Mais próximo à costa, os valores de outono e inverno estão mais próximos, sendo mais variáveis nas profundidades acima de 100 m. Na parte costeira, até 100 m de altitude, área de 11106 km^2, o potencial na primavera foi de 20 GW e no outono 15 GW. A geração ao longo de todo ano na região oceânica seria efetiva se comparada aos valores de geração continental.

A base de observação BOOA, mantem o monitoramento dos fenômenos costeiros e oceânicos. Os dados do LiDAR seguem sendo coletados e poderão ser utilizados em análises futuras sobre a variabilidade do recurso eólico.

Para trabalhos futuros, sugere-se realizar a modelagem até a atualidade, para análises de larga escala, como a possível influência de períodos de El Niño na geração elétrica dos parques brasileiros. Analises dos custos

de implementação de um parque eólico *offshore* no país também somariam aos estudos na área.

Embora os parques eólicos tenham um efeito muito visível na paisagem, seu impacto ambiental é mínimo se planejados de forma sensível. Ao contrário das fontes fósseis e das usinas de energia nuclear, os parques eólicos não precisam de água para resfriamento. As turbinas oceânicas são maiores, sendo necessário uma menor quantidade. Com as fundações de base flutuantes, que estão sendo testadas, os impactos serão menores e poderão estar localizadas em águas mais profundas.

A energia eólica é uma realidade, mas o papel do oceanógrafo está em analisar e incentivar que essa extração ocorra no oceano, protegendo ás áreas costeiras e de preservação. A necessidade do aumento de geração de energia é um fato por isso é preciso otimizar, degradando o menos possível o ambiente. A cada semestre novas ferramentas e tecnologias tem surgido, mostrando que o mercado energético *offshore* só tende a expandir e está próximo de virar realidade na costa brasileira.

REFERÊNCIAS

Amarante O. A. Camargo do; Zack J., Brower M.; Sá A. Leite. Atlas do Potencial Eólico Brasileiro. Brasília, Brasil, Centro de Pesquisas de Energia Elétrica (Cepel). 2001

Archer, C. L., and Coauthors: Meteorology for coastal/offshore wind energy in the United States: Recommendations and research needs for the next 10 years. Bull. American Meteorological Society, 95, 515–519, 2014.

Atlas eólico: Rio Grande do Sul. Elaborado por Camargo Schubert Engenheiros Associados, Eletrosul Centrais Elétricas S.A. Porto Alegre, 2014, 116 p. Disponível em: http://www.eletrosul.gov.br/ les/ les/Desta ques/Atlas_Eolico_Rio_Grande_do_Sul_2014.pdf

Capps, S. B.; Zender, C. S. Global ocean Wind power sensitivity to surface of layer stability. Geophysical Research Letters, Wiley Online Library, v. 36, n. 9, 2009.

Carvalho, D. et al. Offshore winds and wind energy production estimates derived from ASCAT, OSCAT, numerical weather prediction models and buoys−A comparative study for the Iberian Peninsula Atlantic coast. Renewable Energy, v. 102, p. 433-444, 2017.

Cavalcanti, Iracema F. de Albuquerque; FERREIRA, Nelson Jesus; SILVA, Maria Gertrudes A. Justi; DIAS, Maria A. F. da Silva. Tempo e Clima no Brasil. In Portuguese. Oficina e Textos. ISBN 978-85-86238-92-5, São Paulo, 528p, 2009.

CEPAL. Generación e Integración de bases de datos climáticas históricas y de proyecciones de cambio climático para la gestión de riesgos costeros en el estado de Santa Catarina, Brasil, Comissão Econômica para a América Latina e o Caribe. 2015

Colle, B. A., M. J. Sienkiewicz, C. L. Archer, D. E. Veron, F. Veron, and W. Kempton, Improving the mapping and prediction of offshore wind resources (IMPOWR): Experimental overview and first results, Bull. American Meteorological Society, doi:10.1175/BAMS-D-14-00253.1. 2016

Custodio, R. S. Energia Eólica para produção de energia elétrica. 2 ed. rev. e ampl. Rio de Janeiro: Synergia, 2013, 319 p.

Esteban, M. D., Diez, J. J., López, J. S., & Negro, V. Why offshore wind energy? Renewable Energy, 36(2), 444-450. 2011

EPE. Balanço Energético Nacional 2017: Ano base 2016 / Empresa de Pesquisa Energética. – Rio de Janeiro, 2017.

EPE. Plano Decenal de Expansão de Energia 2024. Empresa de Pesquisa Energética. Rio de Janeiro, 2015

Global Wind Energy Council (GWEC)- Global Wind Report- Annual Market Update. 2015

Inger, R., Attrill, M. J., Bearhop, S., Broderick, A. C., James Grecian, W., Hodgson, D. J., Mills, C., Sheehan, E., Votier, S. C., Witt, M. J. and Godley, B. J. (2009), Marine renewable energy: potential benefits to biodiversity? An urgent call for research. Journal of Applied Ecology. 46: 1145–1153. doi:10.1111/j.1365-2664.2009.01697.x 2009.

IPCC- Intergovernmental Panel on Climate Change, Special Report on Renewable Energy Sources and Climate Change Mitigation: Summary for Policymakers and Technical Summary, Intergovernmental Panel on Climate change, Geneva, 2011.

Jacobson, Mark Z. et al. 100% clean and renewable wind, water, and sunlight (WWS) all-sector energy roadmaps for the 50 United States. Energy & Environmental Science, v. 8, n. 7, p. 2093-2117, 2015.

Kaldellis, J.K.; D. Apostolou, M. Kapsali, E. Kondili, Environmental and social footprint of offshore wind energy. Comparison with onshore counterpart, Renewable Energy, Volume 92, July 2016, Pages 543-556, ISSN 0960-1481, http://dx.doi.org/10.1016/j.renene.2016.02.018. 2016

Kempton, W., Archer, C. L., Dhanju, A., Garvine, R. W., & Jacobson, M. Z. Large CO_2 reductions via offshore wind power matched to inherent storage in energy end-uses. Geophysical Research Letters, v. 34, n. 2, 2007.

Manwell, J. F.; Mcgowan, J. G.; Rogers, A. L. Wind Energy Explained: Theory, Design and Application. 2a Edition. ed. Massachusetts: John Wiley & Sons, 705 p., 2009.

Ministério de Minas e Energia. Relatório Mensal do Núcleo de estudos estratégicos de energia. 2016.

Musial, W. BUTTERFIELD, S. Energy from Offshore Wind. National Renewable Energy Laboratory, Colorado, 2006.

Paulson, C. A., The mathematical representation of wind speed and temperature profiles in the unstable atmospheric surface layer. J. Appl.Meteor., 9, 857–861. 1970.

Pryor, S. C.; BARTHELMIE, R. J. Assessing the vulnerability of wind energy to climate change and extreme events. Climatic change, v. 121, n. 1, p. 79-91, 2013.

Sempreviva, A. M., Barthelmie, R. J., & Pryor, S. C. Review of methodologies for offshore wind resource assessment in European seas. Surveys in Geophysics, 29(6), 471-497. 2008.

Silva, Allan Rodrigues et al. Complementarity of Brazilʹs hydro and offshore wind power. Renewable and Sustainable Energy Reviews, v. 56, p. 413-427, 2015.

Steiner, Andrea et al. Critical weather situations for renewable energies–Part A: Cyclone detection for wind power. Renewable Energy, v. 101, p. 41-50, 2017.

ANEXOS

Figura 1- Densidade de potência da costa brasileira nas linhas contínuas pretas em Wm^{-2} e potência de turbina em MW (paleta de cores), representando o Outono (Fall) e Primavera (Spring) respectivamente. Os mapas foram realizados com dados de 1989 a 2009. (Silva et al, 2015).
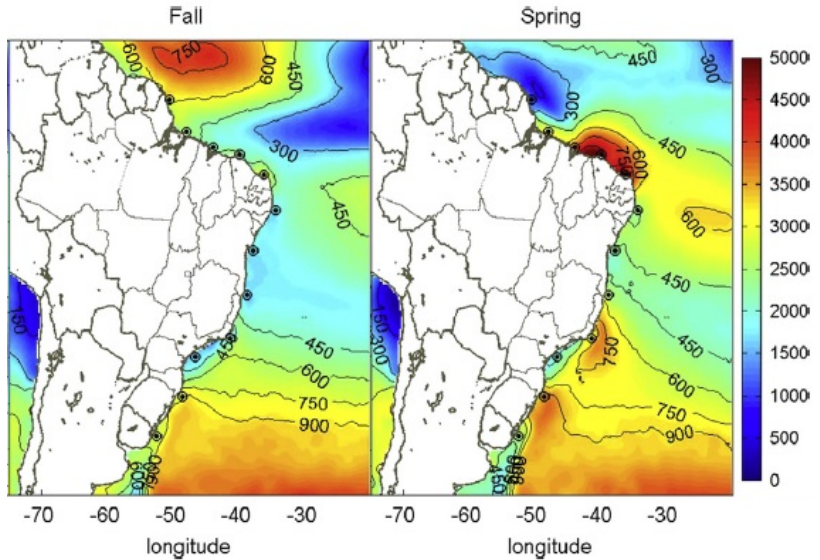
Tabela 1 – Geração elétrica, de 2016, do estado de Santa Catarina, em comparação a Região Sul e ao Brasil e dados de capacidade instalada em 2016 (GW). (Modificada de EPE,2017).

Geração Elétrica		
SC	28.116 GWh	Média: 3.2 GW
SC+PR+RS	171.225 GWh	Média: 19 GW
Brasil	578.898 GWh	Média: 66 GW
Capacidade instalada em 2016		
SC	5.47 GW	
SC+PR+RS	31.685 GW	
Brasil	151.338 GW	

Tabela 2 – Parametrização utilizada na configuração do modelo WRF

Parametrização	Utilizado	Descrição
Modelo de solo e superfície	Noah LSM	NoahLand Surface Model (LSM), divide o solo em 4 camadas de 10, 30, 60 e 100 cm.
Camada Superficial	MM5 Similatity scheme	Desenvolvido por Paulson (1970) e emparelhado com o usado na camada limite.
Camada limite	YSU	Yonsei University PBL sheme, esquema de primeira ordem que utiliza coeficientes de difusão turbulenta para calcular os fluxos turbulentos.
Radiação de onda curta	CAM	Community Atmosphere Model (CAM), inclue tanto onda larga como onda curta.
Radiação de onda longa	CAM	
Microfísica	WSM5	WRF Single-Moment 5
Convecção	Kain-Frisch	Esquema de fluxo de massa

Adaptado de CEPAL (2015)

Tabela 3- Potencial eólico sazonal, com a turbina Vestas 3 MW, nas cotas altimétricas continentais.

	Bathymetric interval	Shelf area (km^2)	Resource (GW)	VE 3.0
LAND	>600m	27459	Summer	50
			Fall	47
			Winter	59
			Spring	58
	0-1000m	54720	Summer	89
			Fall	83
			Winter	98
			Spring	103
	0-600m	27261	Summer	40
			Fall	36
			Winter	39
			Spring	46
	0-100m	11106	Summer	17
			Fall	15
			Winter	16
			Spring	20

Tabela 4- Potencial eólico sazonal, com a turbina Vestas 3 MW, nas batimetrias oceânicas.

	Bathymetric interval	Shelf area (km^2)	Resource (GW)		VE 3.0
OCEAN	0-20m	3870	Summer		9
			Fall		8
			Winter		8
			Spring		10
	0-30m	7002	Summer		16
			Fall		15
			Winter		15
			Spring		19
	0-50m	14976	Summer		39
			Fall		35
			Winter		37
			Spring		45
	0-100m	33714	Summer		96
			Fall		90
			Winter		98
			Spring		112
	0-500m	57663	Summer		176
			Fall		169
			Winter		185
			Spring		206
	0-1000m	59769	Summer		184
			Fall		177
			Winter		194
			Spring		215